MICROSCOPIC CALCULATION OF COLLECTIVE HAMILTONIAN FOR COMPLEX NUCLEI

By

Liyuan Jia

A DISSERTATION

Submitted to
Michigan State University
in partial fulfillment of the requirements
for the degree of

DOCTOR OF PHILOSOPHY

Physics

2012

UMI Number: 3523794

All rights reserved

INFORMATION TO ALL USERS
The quality of this reproduction is dependent on the quality of the copy submitted.

In the unlikely event that the author did not send a complete manuscript
and there are missing pages, these will be noted. Also, if material had to be removed,
a note will indicate the deletion.

UMI 3523794

Copyright 2012 by ProQuest LLC.

All rights reserved. This edition of the work is protected against
unauthorized copying under Title 17, United States Code.

ProQuest LLC.
789 East Eisenhower Parkway
P.O. Box 1346
Ann Arbor, MI 48106 - 1346

ABSTRACT

MICROSCOPIC CALCULATION OF COLLECTIVE HAMILTONIAN FOR COMPLEX NUCLEI

By

Liyuan Jia

A formalism is proposed for microscopic calculation of the collective nuclear Hamiltonian from the underlying nucleonic Hamiltonian, based on the generalized density matrix. It goes beyond the well-known random phase approximation, which calculates only the harmonic terms in the collective Hamiltonian. Many nuclei, including those at the γ-unstable and rotational limits, have a vanishing or negative harmonic potential; there the anharmonic terms calculated by the generalized density matrix method are indispensable restoring the stability of the system. The proposed formalism is tested in several models by comparing with the exact results. Realistic applications on tin isotopes are discussed.

ACKNOWLEDGMENT

I gratefully express many thanks to my advisor Vladimir Zelevinsky. He helped me in his best to grow as a physicist, starting from an engineering undergraduate major. His understanding for the student, especially during the difficult times, makes my PhD years an enjoyable journey.

I am grateful to people at the cyclotron and the physics department. It is a very good working environment here. I received numerous help from professors, staff members, and fellow students here. Without them, it would be impossible to finish this work.

Support from friends is always important. It is fortunate for me to meet some new friends here at MSU; I believe our friendship will continue.

At last, thanks to my parents for their support, as always.

TABLE OF CONTENTS

LIST OF TABLES

LIST OF FIGURES

Chapter 1

Introduction

The nuclear many-body problem aims at describing a nucleus in terms of nucleonic degrees of freedom. It is very difficult in at least two aspects. First, the interaction between nucleons, as the residual force among their quark components, is still not firmly established. Second, exact solution is impossible except for very light nuclei, as is common in many-body physics. The non-perturbative nature of nucleon force makes the nuclear problem particularly difficult.

Until now the most effective treatment starts from a self-consistent mean field, generated by the participating nucleons themselves. In the first step, nucleons move independently in the mean field obeying the Fermi statistics. In the next step, the nucleons interact with each other through the residual force that is not included into the mean field. The standard treatment is given by the nuclear shell model (configuration interaction). There the residual interaction is diagonalized in a huge many-body space that consists of Slater determinants built of single-particle levels. However, the dimension of the space makes it impractical in cases of many active nucleons in lots of relevant single-particle levels, which is typical for medium and heavy nuclei.

The collective motion is an important type of dynamics in nuclei. Intuitively, it can be thought of as the motion of the nucleus as a whole, such as vibration and rotation, where many nucleons move coherently (in phase). Typical features of the collective states are their low excitation energies and large transition rates. For these collective states, another type of description using an effective bosonic Hamiltonian is successful, including the well-known geometric Bohr Hamiltonian [1, 2] and interacting boson model [3]. Broad sets of nuclear data are described with a few parameters that change smoothly across the nuclear chart. This shows that, out of the huge Slater-determinant space, there exist a few collective degrees of freedom, which are usually sufficient for describing the low-lying collective states. To put the phenomenological theory on solid grounds, serious efforts were devoted to calculating these parameters microscopically from the underlying nucleonic Hamiltonian. But the complete theory is still missing after several decades.

The purpose of this thesis is the microscopic calculation of the collective/bosonic Hamiltonian by the generalized density matrix (GDM) method. This method was proposed long ago [4, 5, 6] and was applied to nuclear rotation [5, 7, 8] and large-amplitude collective motion [9, 10, 11]. Here the construction is considered in the most general way. As a result, the whole nuclear chart, from vibrational, through γ-unstable, to rotational regions, can be described on the same footing. From another perspective, the approach greatly generalizes the well-known random phase approximation (RPA). The lowest orders of the GDM method give naturally Hartree-Fock (HF) equations and RPA; higher orders fix the anharmonic terms in the collective Hamiltonian. Only near the closed shells, where the RPA frequency ω^2 is large, the harmonic potential term dominates and the RPA is a good approximation. Going away from closed shells, ω^2 becomes small and finally negative. There the anharmonic terms

are indispensable restoring the stability of the system.

The thesis is organized as following. In chapter 2 we present the GDM formalism in the simplest scenario, without complications owing to angular-momentum vector coupling. The validity of the GDM method is then examined in chapter 3 by comparing with the exact shell-model results in several models. Chapter 4 is devoted to applications for a realistic nuclear system with rotational symmetry and pairing. Finally, we consider in chapter 5 a specific Hamiltonian – the quadrupole plus pairing Hamiltonian, with realistic calculations for tin isotopes. Some details of the calculations are given in Appendices. The results are partly published [12, 13, 14].

Chapter 2

Generalized Density Matrix Method

In this chapter we review the essence of the GDM method in simple systems without complications owing to rotational symmetry and pairing correlations. A single collective mode is assumed; the case of multiple modes is discussed briefly in Appendix D.

2.1 Development

The starting point is the microscopic fermionic Hamiltonian

$$H = \sum_{12} \epsilon_{12} a_1^\dagger a_2 + \frac{1}{4} \sum_{1234} V_{1234} a_1^\dagger a_2^\dagger a_3 a_4. \tag{2.1}$$

Here the operators of single-particle energy ϵ and residual interaction V are expressed using an arbitrary basis. We find it convenient for H, ϵ_{12} and V_{1234} to be dimensionless; in other words H is measured in some unit of energy. We have assumed in Eq. (2.1) a two-body force, inclusion of three-body forces is discussed in Appendix A of Ref. [12]. In accordance with the discussion in Introduction, we consider a typical case when the system described by the

Hamiltonian (2.1) has a band of collective states $\{|C_i\rangle\}$, characterized by low energies and large transition rates. We assume that there exists a reference state $|\Phi\rangle$, a collective mode operator $A^\dagger = (u\alpha + iv\pi)/\sqrt{2}$ ($uv = -1$, α and π are collective coordinate and momentum), such that *approximately*

$$[\alpha, \pi] = i, \tag{2.2}$$

$$|C_i\rangle = [\ c_{i0} + c_{i1}A^\dagger + c_{i2}(A^\dagger)^2 + \dots\ ]\ |\Phi\rangle, \tag{2.3}$$

$$\begin{aligned}\langle C_i|\ H\ |C_j\rangle = \langle C_i|\ E_0 + \frac{\omega^2}{2}\ \alpha^2 + \frac{1}{2}\ \pi^2 + \frac{\Lambda^{(30)}}{3!}\ \alpha^3 + \frac{\Lambda^{(12)}}{4}\ \{\alpha, \pi^2\} \\ + \frac{\Lambda^{(40)}}{4!}\ \alpha^4 + \frac{\Lambda^{(22)}}{8}\ \{\alpha^2, \pi^2\} + \frac{\Lambda^{(04)}}{4!}\ \pi^4 + \dots\ |C_j\rangle.\end{aligned} \tag{2.4}$$

Eq. (2.2) says that $A^\dagger$ is effectively a boson operator. Eq. (2.3) says that the collective band $\{|C_i\rangle\}$ can be built by repeated action of $A^\dagger$ on the reference state $|\Phi\rangle$. Later $|\Phi\rangle$ will be identified as the HF ground state. Eq. (2.4) says that within the band, the effect of the fermionic Hamiltonian (2.1) can be approximated by an expansion over the bosonic operators, where all time-even terms are kept (α is time-even, π is time-odd). The curly brackets represent anti-commutator, $\{A, B\} \equiv AB + BA$.

The generalized density matrix operator is defined as

$$R_{12} \equiv a_2^\dagger a_1. \tag{2.5}$$

Similarly to Eq. (2.4), we assume that within the band the effect of R can be approximated

by a boson expansion

$$\langle C_i|R_{12}|C_j\rangle = \langle C_i|\ \rho_{12} + r_{12}^{(10)}\alpha + r_{12}^{(01)}\pi + r_{12}^{(20)}\frac{\alpha^2}{2} + r_{12}^{(02)}\frac{\pi^2}{2} + r_{12}^{(11)}\frac{\{\alpha,\pi\}}{2} + r_{12}^{(30)}\frac{\alpha^3}{3!} + r_{12}^{(03)}\frac{\pi^3}{3!} + r_{12}^{(21)}\frac{\{\alpha^2,\pi\}}{4} + r_{12}^{(12)}\frac{\{\alpha,\pi^2\}}{4} + \ldots\ |C_j\rangle. \tag{2.6}$$

The expansion coefficients $r^{(mn)}$ are called generalized density matrices. They are matrices in the single-particle space and do not act in the band of collective states. Later the constant term ρ in Eq. (2.6) will be identified as the usual density matrix on the HF ground state. Terms with operators α and π generate interaction within the band.

The exact equation of motion for the density matrix operator in the full many-body Hilbert space is

$$[R_{12}, H] = [\epsilon, R]_{12} - \frac{1}{2}\sum_{345} V_{5432}a_5^\dagger a_4^\dagger a_3 a_1 + \frac{1}{2}\sum_{345} V_{1345}a_2^\dagger a_3^\dagger a_4 a_5, \tag{2.7}$$

where $[\epsilon, R]_{12} = \sum_3(\epsilon_{13}R_{32} - R_{13}\epsilon_{32})$. Now we map Eq. (2.7) onto the collective subspace, namely, we take matrix elements of Eq. (2.7) between two collective states on both sides. Thus R_{12} and H in Eq. (2.7) can be substituted by their boson expansions (2.6) and (2.4). For the two-body density matrix operator, we assume

$$\langle C_i|\ a_4^\dagger a_3^\dagger a_2 a_1\ |C_j\rangle = \langle C_i|\ a_4^\dagger a_1 \cdot a_3^\dagger a_2 - a_4^\dagger a_2 \cdot a_3^\dagger a_1\ |C_j\rangle, \tag{2.8}$$

that is, it factorizes into antisymmetrized products of one-body density matrix operators within the band. The constant terms (without operators α and π) in Eq. (2.8), $\rho_{1234} = \rho_{14}\rho_{23} - \rho_{24}\rho_{13}$, is routinely used to derive the time-dependent Hartree-Fock equation. The

validity of Eq. (2.8) was studied in detail in Ref. [12]. Substituting Eq. (2.8) into Eq. (2.7) we get the equation of motion in the collective band

$$[R_{12}, H] \stackrel{\circ}{=} [\epsilon + W\{R\}, R]_{12}, \tag{2.9}$$

where "$\stackrel{\circ}{=}$" means projecting onto the collective subspace (taking matrix elements $\langle C_i|...|C_j\rangle$). The generalized self-consistent field is defined as

$$W\{R\}_{12} \equiv \sum_{34} V_{1432} R_{34}. \tag{2.10}$$

On the left-hand side of Eq. (2.9), the intermediate states (between R_{12} and H) are restricted to those of the collective subspace, assuming large transition amplitudes.

For conciseness we rewrite Eq. (2.4) in compact form,

$$H \stackrel{\circ}{=} \sum_{m\geq 0, l\geq 0}^{m+2l\geq 2} \Lambda^{(m,2l)} \ \frac{1}{2}\frac{\{\alpha^m, \pi^{2l}\}}{m!(2l)!}, \tag{2.11}$$

where $\Lambda^{(20)} = \omega^2$, $\Lambda^{(02)} = 1$. Similarly Eq. (2.6) is rewritten as

$$R_{12} \stackrel{\circ}{=} \sum_{m\geq 0, n\geq 0} r_{12}^{(mn)} \ \frac{1}{2}\frac{\{\alpha^m, \pi^n\}}{m!\, n!}. \tag{2.12}$$

The substitution of Eq. (2.12) into Eq. (2.10) gives the mapping of the latter,

$$W\{R\} \stackrel{\circ}{=} \sum_{mn} w^{(mn)} \ \frac{1}{2}\frac{\{\alpha^m, \pi^n\}}{m!\, n!}, \tag{2.13}$$

where $w^{(mn)} \equiv W\{r^{(mn)}\}$.

Substituting Eqs. (2.11) and (2.12) into Eq. (2.9), on the left-hand side we calculate commutators such as $[\alpha^2, \pi] = 2i\alpha$. Then, comparing coefficients with the same operator structure, we come to the final set of GDM equations with different $r \geq 0$, $s \geq 0$,

$$\sum_{0\leq p(\leq r+1),0\leq 2l(\leq s+1)}^{p+2l\geq 2} \frac{2l(r+1-p)-(s+1-2l)p}{(r+1-p)!\ (s+1-2l)!\ p!\ (2l)!} \cdot i\ \Lambda^{(p,2l)} r^{(r+1-p,s+1-2l)}$$
$$= \frac{1}{r!\ s!}\ [\epsilon, r^{(rs)}] + \sum_{0\leq p(\leq r),0\leq q(\leq s)} \frac{1}{(r-p)!\ (s-q)!\ p!\ q!}\ [w^{(r-p,s-q)}, r^{(pq)}]. \qquad (2.14)$$

2.2 Hartree-Fock Equation

Equation (2.14) with $(rs) = (00)$ gives

$$0 = [\epsilon + W\{\rho\}, \rho]. \qquad (2.15)$$

Thus $f \equiv \epsilon + W\{\rho\}$ and ρ can be diagonalized simultaneously in some single-particle basis:

$$f_{12} = \delta_{12} e_1, \quad \rho_{12} = \delta_{12} n_1, \qquad (2.16)$$

providing mean-field single-particle energies e_1 and occupation numbers n_1. In what follows, we will always use this single-particle basis. If we restrict the reference state $|\Phi\rangle$ to be a Slater determinant, then the occupation numbers n_1 can be only 0 or 1; in this case Eq. (2.15) is the usual HF equation, $|\Phi\rangle$ is the HF ground state. More general choices, such as the thermal ensemble, are also possible. For future convenience we define

$$e_{12} \equiv e_1 - e_2, \quad n_{12} \equiv n_1 - n_2. \qquad (2.17)$$

We assume that degenerate single-particle levels have the same occupancies,

$$e_1 = e_2 \;\Rightarrow\; n_1 = n_2, \tag{2.18}$$

but the reverse is not necessarily true.

2.3 Random-Phase Approximation

Equation (2.14) with $(rs) = (10), (01)$ gives

$$ir^{(10)} = [f, r^{(01)}] + [w^{(01)}, \rho], \tag{2.19}$$

$$-i\omega^2 r^{(01)} = [f, r^{(10)}] + [w^{(10)}, \rho], \tag{2.20}$$

where $w^{(10)} = W\{r^{(10)}\}$, and $w^{(01)} = W\{r^{(01)}\}$ are the corresponding components of the self-consistent field. This is the set of RPA equations. The formal solution is

$$r_{12}^{(10)} = \frac{n_{12}}{(e_{12})^2 - \omega^2}[-i\omega^2\ w_{12}^{(01)} + e_{12} w_{12}^{(10)}], \tag{2.21}$$

$$r_{12}^{(01)} = \frac{n_{12}}{(e_{12})^2 - \omega^2}[i\ w_{12}^{(10)} + e_{12} w_{12}^{(01)}]. \tag{2.22}$$

Note that $r^{(10)}$ and $r^{(01)}$ have only $n_1 \neq n_2$ matrix elements. From Eqs. (2.10), (2.21) and (2.22) we obtain a linear homogenous set of equations for $w^{(10)}$ and $w^{(01)}$:

$$w_{34}^{(10)} = \sum_{12} V_{3214} \frac{n_{12}}{(e_{12})^2 - \omega^2}[-i\omega^2 w_{12}^{(01)} + e_{12} w_{12}^{(10)}], \tag{2.23}$$

$$w_{34}^{(01)} = \sum_{12} V_{3214} \frac{n_{12}}{(e_{12})^2 - \omega^2}[i w_{12}^{(10)} + e_{12} w_{12}^{(01)}]. \tag{2.24}$$

A non-zero solution requires a zero determinant, from which we solve for the harmonic frequency ω^2. The lowest solution should be taken corresponding to the collective motion.

2.4 Higher Orders

For $K = r + s \geq 1$ in Eq. (2.14), we solve a linear set of coupled equations for $r^{(rs)}|_{r+s=K}$ in terms of lower-order quantities. The formal solution can be written as

$$\begin{aligned} r^{(mn)}|_{m+n=K} = & - \sum_{r+s=K} \sum_{0\leq p(\leq r+1),0\leq 2l(\leq s+1)}^{p+2l\geq 3} \frac{2l(r+1-p)-(s+1-2l)p}{(r+1)(s+1)} \\ & \cdot C^p_{r+1} C^{2l}_{s+1}\ i\ \Lambda^{(p,2l)} \cdot \eta^{(mn)}_{(rs)} : r^{(r+1-p,s+1-2l)} \\ & + \sum_{r+s=K} \sum_{0\leq p(\leq r),0\leq q(\leq s)}^{p+q\leq r+s-1} C^p_r C^q_s \cdot \eta^{(mn)}_{(rs)} : [w^{(r-p,s-q)}, r^{(pq)}], \end{aligned} \tag{2.25}$$

where $C^q_p = p!/[q!(p-q)!]$, and we have introduced the "weight" matrix $\eta^{(mn)}_{(rs)}$ so that $(\eta^{(mn)}_{(rs)} : r)_{12} = \eta^{(mn)}_{(rs)12} r_{12}$. The matrix η is given by

$$\eta^{(mn)}_{(rs)} = (D^{-1}_K)^{(rs)}_{(mn)}, \tag{2.26}$$

where D_K is a tridiagonal matrix of dimension $K+1$, with non-vanishing matrix elements

$$\begin{aligned} (D_K)^{(mn)}_{(mn)} &= -e, \\ (D_K)^{(m+1,n-1)}_{(mn)} &= i \cdot n, \\ (D_K)^{(m-1,n+1)}_{(mn)} &= -i \cdot \omega^2 m. \end{aligned} \tag{2.27}$$

We give as an example the D and η matrices in the lowest two orders. For $K = 1$,

$$D^{(mn)}_{(rs)} = \left(\begin{array}{c|cc} (mn)\setminus(rs) & (01) & (10) \\ \hline (01) & -e & -i\omega^2 \\ (10) & i & -e \end{array}\right), \tag{2.28}$$

from which we solve by Eq. (2.26)

$$\eta^{(mn)}_{(rs)} = \frac{1}{e^2-\omega^2}\cdot\left(\begin{array}{c|cc} (mn)\setminus(rs) & (01) & (10) \\ \hline (01) & -e & -i \\ (10) & i\omega^2 & -e \end{array}\right). \tag{2.29}$$

Hence the RPA solutions (2.21) and (2.22) are rederived substituting the above expression into Eq. (2.25). For $K = 2$,

$$D^{(mn)}_{(rs)} = \left(\begin{array}{c|ccc} (mn)\setminus(rs) & (02) & (11) & (20) \\ \hline (02) & -e & -i\omega^2 & 0 \\ (11) & 2i & -e & -2i\omega^2 \\ (20) & 0 & i & -e \end{array}\right), \tag{2.30}$$

from which we solve by Eq. (2.26)

$$\eta^{(mn)}_{(rs)} = \frac{1}{-e(e^2-4\omega^2)}\cdot\left(\begin{array}{c|ccc} (mn)\setminus(rs) & (02) & (11) & (20) \\ \hline (02) & e^2-2\omega^2 & 2ie & -2 \\ (11) & -i\omega^2 e & e^2 & ie \\ (20) & -2\omega^4 & -2i\omega^2 e & e^2-2\omega^2 \end{array}\right). \tag{2.31}$$

From Eq. (2.31) we read, for example, $\eta^{(20)}_{(02)12} = \{-2\omega^4\}/\{-e_{12}[(e_{12})^2 - 4\omega^2]\}$, where 1 and 2 are single-particle indices. All η matrices with an *even* K have the factor $1/e$ [see for example Eq. (2.31)], thus the $e_1 = e_2$ matrix elements of $r^{(mn)}_{12}$ cannot be directly calculated from the solutions (2.25). However, if we set $n_1 = n_2$ in Eq. (2.25) and simplify, the $1/e_{12}$ divergence is canceled; the resulting expression is used to calculate $r^{(mn)}_{12}$. The $e_1 = e_2$ matrix elements of $r^{(mn)}_{12}$ are expressed in terms of lower-order quantities.

In each order K, substituting $r^{(mn)}$ from Eq. (2.25) into $w^{(mn)}_{12} = \sum_{34} V_{1432} r^{(mn)}_{34}$ results in a linear set of coupled equations for the latter, from which the $e_1 \neq e_2$ matrix elements of $w^{(mn)}_{12}$ are solved in terms of lower-order quantities, which in turn gives the $e_1 \neq e_2$ matrix elements of $r^{(mn)}_{12}$ by Eq. (2.25). However, if $K = 2L + 1$ is odd, the determinant for $w^{(mn)}$ is zero. This can be proved as following. Summing Eq. (2.14) with proper weights we get

$$\begin{aligned} i\ x &= [W\{y\}, \rho] + [f, y] + \ldots, \\ -i\ \omega^2 y &= [W\{x\}, \rho] + [f, x] + \ldots, \end{aligned} \tag{2.32}$$

where

$$\begin{aligned} x &= \sum_{0 \le t \le L} \frac{\nu_t}{(2t+1)!\ (2L-2t)!}\ r^{(2t+1, 2L-2t)}, \\ y &= \sum_{0 \le t \le L} \frac{\mu_t}{(2t)!\ (2L+1-2t)!}\ r^{(2t, 2L+1-2t)}, \end{aligned}$$

in which μ_t and ν_t are solved from ($0 \le t \le L$, $\mu_{L+1} = \nu_{-1} = 0$)

$$\begin{aligned} -\frac{2L-2t}{2t+1}\ \omega^2 \mu_{t+1} + \mu_t &= \frac{1}{2t+1}\ \nu_t, \\ \omega^2 \nu_t - \frac{2t}{2L-2t+1}\ \nu_{t-1} &= \frac{1}{2L+1-2t}\ \omega^2 \mu_t. \end{aligned}$$

The "..." in Eq. (2.32) are lower-order quantities. It is seen that the explicitly shown parts of Eq. (2.32) have the same structure as the RPA equations (2.19) and (2.20). This finishes the proof. The zero determinant means that the set of equations for $w^{(mn)}$ is linearly dependent, and there is a constraint in each order of odd K, entering as a solvability condition. These constraints are the main results of the GDM formalism, from which the parameters $\Lambda^{(pq)}$ of the collective Hamiltonian are calculated. Then $w^{(mn)}$ is solved from this zero-determinant set, with only a factor undetermined. This factor is fixed by the constraint indicated in the next section below Eq. (2.33).

2.5 Self-consistent Hamiltonian Condition

If the GDM formalism is self-consistent, the substitution of the solutions (2.25) into Eq. (2.1) should reproduce the assumed Hamiltonian (2.11),

$$\Lambda^{(mn)} = \mathrm{Tr}\,[\epsilon r^{(mn)}] + \frac{1}{2} \sum_{0\leq p(\leq m),0\leq q(\leq n)} C_m^p C_n^q \ \mathrm{Tr}[r^{(pq)} w^{(m-p,n-q)}]. \tag{2.33}$$

In an order of odd $K = m + n$, all the parameters $\Lambda^{(mn)}$ are checked correctly. In an order of even $K = m + n$, all but one $\Lambda^{(mn)}$ are checked correctly; this one leftover degree-of-freedom/constraint is used to fix the remaining "undetermined factor" mentioned at the end of the last section.

2.6 Equivalent Representations of Collective Hamiltonian

We have shown in Sec. 2.4 that in each even order in the collective Hamiltonian the GDM method gives one constraint (in the harmonic order it is the RPA secular equation). In this section we show that these constraints fix the collective Hamiltonian (2.4) completely. In Eq. (2.4) all terms with the right symmetry are kept thus the expansion is complete. However, in fact it is over-complete. Different expansions are equivalent if they are related by canonical transformations of collective variables α and π. The number of independent parameters of H should be equal to the number of possible combinations as in Eq. (2.4) minus the number of allowed transformations.

Microscopic estimates of quite general type [15] show that $\Lambda^{(mn)} \sim \Omega^{-(m+n-2)/2}$, where Ω is the collectivity factor, the effective number of simple quasiparticle excitations contributing to the collective mode. The solvable Lipkin model and quadrupole plus pairing model confirm these estimates [12]. In the case of strong collectivity, $\Omega \gg 1$.

Let us count the number of transformations $(\alpha, \pi) \to (\bar{\alpha}, \bar{\pi})$,

$$\begin{aligned} \alpha &= \sum_{m\geq 0, n\geq 0} x^{(mn)} \ \frac{1}{2}\frac{\{\bar{\alpha}^m, \bar{\pi}^n\}}{m!\ n!} \ , \\ \pi &= \sum_{m\geq 0, n\geq 0} y^{(mn)} \ \frac{1}{2}\frac{\{\bar{\alpha}^m, \bar{\pi}^n\}}{m!\ n!} \ , \end{aligned} \tag{2.34}$$

which preserve the commutator algebra,

$$[\alpha, \pi] = [\bar{\alpha}, \bar{\pi}] = i. \tag{2.35}$$

The transformation parameters $x^{(mn)}, y^{(mn)}$ being of the order $\Omega^{-(m+n-1)/2}$ will not change the dependence of $\Lambda^{(mn)}$ in Eq. (2.4) on Ω. The constant terms, $x^{(00)}$ and $y^{(00)}$, corresponding to a trivial translation of origin are not needed as this choice is already made by selecting $\Lambda^{(10)} = \Lambda^{(01)} = 0$ in the collective Hamiltonian (2.4); in the case of a multipole collective mode such terms would violate rotational symmetry. In the linear terms we can set $x^{(10)} = y^{(01)} = 1$, which would correspond to a rescaling of α or π [$\Lambda^{(02)} = 1$ in Eq. (2.4)]. The parameters $x^{(mn)}$ and $y^{(mn)}$ vanish for odd and even n, respectively, because of the wrong time-reversal symmetry.

Using Eqs. (2.34) and (2.35) we have

$$[\alpha, \pi] = \frac{i}{2} \sum_{rsmn} x^{(mn)} y^{(r-m,s-n)} \cdot \frac{[m(s-n) - n(r-m)]}{m!\ n!\ (r-m)!\ (s-n)!}\ \{\bar{\alpha}^{r-1}, \bar{\pi}^{s-1}\}, \tag{2.36}$$

where in the coefficient of $\{\bar{\alpha}^{r-1}, \bar{\pi}^{s-1}\}$ we keep only the leading terms in $1/\Omega$, that is, terms $\sim \Omega^{-(r+s-2)/2}$. The summation runs over $r \geq m$ and $s \geq n$, and as seen from the numerator, $r \geq 1$ and $s \geq 1$. In addition, s is odd, otherwise $x^{(mn)} y^{(r-m,s-n)}$ vanishes. The starting term, $r = s = 1$, gives correctly i. The terms with $r + s \geq 3$ and an odd s should vanish,

$$0 = \sum_{mn} x^{(mn)} y^{(r-m,s-n)}\ \frac{m(s-n) - n(r-m)}{m!\ n!\ (r-m)!\ (s-n)!}. \tag{2.37}$$

These relations constrain $x^{(mn)}$ and $y^{(mn)}$ in the transformations (2.34).

Let us identify the independent parameters in the collective Hamiltonian (2.4), removing the redundant degrees of freedom related to the transformations (2.34). In the quadratic order, the transformations (2.34) do not change the harmonic terms $\frac{\omega^2}{2}\alpha^2 + \frac{1}{2}\pi^2$; thus,

there is one independent parameter ω^2. In the cubic order, the transformations (2.34) with nonzero $x^{(20)}$, $x^{(02)}$, and $y^{(11)}$ influence the Hamiltonian parameters $\Lambda^{(30)}$ and $\Lambda^{(12)}$ through the harmonic terms; there is one constraint (2.37) with $(rs) = (21)$. Thus, the renormalization of the collective variables removes the skew terms: $\Lambda^{(30)}$ and $\Lambda^{(12)}$ can be set to zero and there remains no independent parameter in this order. In the quartic order, the transformations (2.34) with nonzero $x^{(30)}$, $x^{(12)}$, $y^{(21)}$, and $y^{(03)}$ influence $\Lambda^{(40)}$, $\Lambda^{(22)}$, and $\Lambda^{(04)}$; and there are two constraints (2.37) with $(rs) = (31)$ and (13). Thus, there is one independent parameter; we can, for example, choose it to be $\Lambda^{(40)}$, and set $\Lambda^{(22)}$ and $\Lambda^{(04)}$ to zero.

This process continues to anharmonic terms of higher orders. There is one independent parameter in each even order (we can choose it to be $\Lambda^{(n0)}$ excluding all momentum-dependent high-order terms), and there are no independent parameters in odd orders. In summary, the independent parameters in the collective Hamiltonian (2.4) can be identified in the following form:

$$\begin{aligned} H &= \frac{1}{2}\pi^2 + V(\alpha^2) \ , \\ V(\alpha^2) &= \omega^2 \frac{\alpha^2}{2} + \Lambda^{(40)} \frac{\alpha^4}{4!} + \Lambda^{(60)} \frac{\alpha^6}{6!} + \Lambda^{(80)} \frac{\alpha^8}{8!} + \dots . \end{aligned} \tag{2.38}$$

We have shown in Sec. 2.4 that the GDM method gives one constraint in each even order of anharmonicity, thus fixes all the independent parameters in Eq. (2.38). In this sense the collective Hamiltonian is completely determined.

In practical applications, Eq. (2.38) may not be the most convenient choice for the independent parameters of the collective Hamiltonian, which means solving the equations of motion in the GDM method to infinitely high orders. Alternatively, we can pick up a certain

number (labeled N) of terms in Eq. (2.4), putting other terms to zero; in other words, we *assume* that the original fermionic Hamiltonian (2.1) can be sufficiently accurately mapped onto a collective Hamiltonian with these N terms. Then in the GDM method we need to solve the equations of motion up to the $(2N)^{\rm th}$ order, in order to get N constraints. The quality of the assumption of mapping can be checked self-consistently within the GDM method: if the assumption is good, constraints from the orders higher than $2N$ should be satisfied automatically. For the realistic nucleonic Hamiltonian, mapping onto a bosonic Hamiltonian is guaranteed by the success of numerous phenomenological studies. The mapped quadrupole phonon α_μ is not necessarily the RPA phonon that is "proportional" to the real quadrupole operator Q_μ; rather α_μ is such a renormalized operator (2.34) that the mapping onto a given form (the selected N terms) of the bosonic Hamiltonian is the "best". The possibly infinite series of the bosonic Hamiltonian expanded in the RPA phonon is "pushed"/resummed into the selected finite-N terms by the renormalization (2.34). The expansion of the real quadrupole operator Q_μ in terms of α_μ and π_μ is obtained by substituting the solution (2.12) into $Q_\mu = {\rm Tr}[q_\mu R]$ as shown in the next section.

2.7 Transition Rates

Let us consider the calculation of the transition rates for a one-body operator

$$Q = \sum_{12} q_{12} a_1^\dagger a_2 = {\rm Tr}[qR]. \tag{2.39}$$

The boson expansion of Q is calculated by substituting the solution (2.12) into Eq. (2.39),

$$Q \doteq \sum_{m\geq 0, n\geq 0} \mathrm{Tr}[qr^{(mn)}] \; \frac{1}{2}\frac{\{\alpha^m, \pi^n\}}{m!\, n!} \equiv \sum_{m\geq 0, n\geq 0} Q^{(mn)} \; \frac{1}{2}\frac{\{\alpha^m, \pi^n\}}{m!\, n!}. \tag{2.40}$$

The transition rates of Eq. (2.40) between eigenstates of the bosonic Hamiltonian (2.11) should reproduce that of Eq. (2.39) between eigenstates of the nucleonic Hamiltonian (2.1).

Chapter 3

Validity of the Formalism

In this chapter we examine the validity of the GDM formalism by comparing its results with that of the exact shell-model diagonalization. First we consider the well-known Lipkin model that is analytically solvable. Next we consider models with factorizable forces numerically. As will be shown, the GDM method reproduces the exact results quite well, for both energies and transition rates, through the whole parameter space going from vibrational, γ-unstable to deformed regions.

3.1 Lipkin Model

The Lipkin model [16] is widely used as a test ground for methods of collective motion. In this model, there are two single-particle levels with energies $\pm 1/2$ (the spacing is the energy unit), each with degeneracy Ω. The model Hamiltonian contains only "vertical" transitions

($\sigma = \pm 1$; $l = 1, 2, ..., \Omega$):

$$H = \sum_{\sigma,l} \frac{\sigma}{2} a^{\dagger}_{\sigma,l} a_{\sigma,l} + \frac{\kappa}{2} \sum_{\sigma,l,l'} a^{\dagger}_{\sigma,l} a^{\dagger}_{\sigma,l'} a_{-\sigma,l'} a_{-\sigma,l}. \tag{3.1}$$

There are Ω particles; thus without interaction the lower levels ($\sigma = -1$) are completely filled and the upper levels ($\sigma = 1$) are empty.

We follow Ref. [17] to get the analytical solution. It is easy to show that the quasi-spin operators,

$$J_+ = J^{\dagger}_- = J_x + iJ_y = \sum_l a^{\dagger}_{+1,l} a_{-1,l}, \quad J_z = \frac{1}{2} \sum_{\sigma,l} \sigma a^{\dagger}_{\sigma,l} a_{\sigma,l}, \tag{3.2}$$

satisfy the angular momentum algebra. Using Eq. (3.2) the Hamiltonian (3.1) is written as

$$H = J_z + \frac{1}{2}\kappa(J^2_+ + J^2_-). \tag{3.3}$$

Thus the total quasi-spin J is a good quantum number. With the Holstein-Primakoff transformation,

$$J_+ = J^{\dagger}_- = -i\ A^{\dagger}\sqrt{2J - A^{\dagger}A}, \quad J_z = -J + A^{\dagger}A, \tag{3.4}$$

where $A^{\dagger}$ and A are bosonic creation and annihilation operators with commutation relation $[A, A^{\dagger}] = 1$, the Hamiltonian (3.3) is written as an expansion over $A^{\dagger}$ and A; or collective coordinate α and momentum π by the canonical transformation

$$A = \frac{1}{\sqrt{2}}(u\alpha - iv\pi),\ A^{\dagger} = \frac{1}{\sqrt{2}}(u\alpha + iv\pi),\ uv = -1. \tag{3.5}$$

Assuming strong collectivity $J \gg 1$, we keep only the leading order in $1/J$. Under the choice

$$u \approx \sqrt{1+2\kappa J}, \quad v = -\frac{1}{u}, \tag{3.6}$$

the Hamiltonian becomes

$$H = \frac{\omega^2}{2}\,\alpha^2 + \frac{1}{2}\,\pi^2 + \frac{\Lambda^{(40)}}{4}\,\alpha^4 + \frac{\Lambda^{(04)}}{4}\,\pi^4, \tag{3.7}$$

with

$$\omega^2 \approx 1 - 4\kappa^2 J^2, \quad \Lambda^{(40)} \approx \kappa u^4, \quad \Lambda^{(04)} \approx -\kappa v^4. \tag{3.8}$$

Other $\Lambda^{(mn)}$ vanishes in their leading order of $1/J$.

For the ground-state band, the quantum number J is found from Eq. (3.2):

$$J = |J_z|_{\max} = \frac{\Omega}{2}. \tag{3.9}$$

Using Eqs. (3.6) and (3.9) the result (3.8) can be written as

$$\omega^2 \approx 1 - (\kappa\Omega)^2, \quad \Lambda^{(40)} \approx 6\kappa(1+\kappa\Omega)^2, \quad \Lambda^{(04)} \approx \frac{-6\kappa}{(1+\kappa\Omega)^2}. \tag{3.10}$$

Equations (3.10) are accurate in the leading order of $1/\Omega$.

Now we apply the GDM formalism to the Hamiltonian (3.1). By going up to the sixth

order in the equation of motion, we get three constraints to fix ω^2, $\Lambda^{(40)}$, and $\Lambda^{(04)}$; they agree with the exact results (3.10). Constraints from the eighth order and higher are satisfied identically. Hence, the GDM method solves the Lipkin model completely in the leading order of $1/\Omega$.

In order to compare directly the GDM results with the exact ones, we perform a numerical example at $\Omega = 30$. The results are shown in Fig. 3.1. As one can see, the first few excited states of the anharmonic Hamiltonian agree very well with the exact results, while the RPA fails very soon as κ increases to the critical point (RPA $\omega^2 = 0$). For realistic medium and heavy even-even nuclei, only in the vicinity of magic numbers the low-lying collective excitations can be sufficiently described by the QRPA; in very many cases, including the soft-spherical, γ-unstable, and rotational dynamics, the collective modes lie near or beyond the critical point of QRPA, so that the higher-order anharmonicities in the collective Hamiltonian are indispensable.

In Fig. 3.1, as conventionally done, the bosonic Hamiltonian (3.10) is diagonalized in the infinite phonon space $\{|0 \leq n < +\infty\rangle\}$ ($|n\rangle$ is the state with n phonons, $A^\dagger A|n\rangle = n|n\rangle$), dropping the "divergent" $\Lambda^{(04)} < 0$ term. However, as discussed in Ref. [12], the Hamiltonian (3.10) should really be diagonalized in the finite physical space $\{|0 \leq n \leq \Omega\rangle\}$. Acting $A^\dagger$ more than Ω times on the ground state runs out of valence particles thus gives zero. Similar phenomena should exist in realistic nuclei, when the relevant particles (holes) near the Fermi surface are exhausted by repeated actions of the phonon creation operator $A^\dagger$. In the GDM method we need to determine the parameter u in $A^\dagger$ (3.5). It is fixed by minimizing $A|\Phi\rangle$ in its one-particle-one-hole components, where $|\Phi\rangle$ is the Hartree-Fock ground state that is

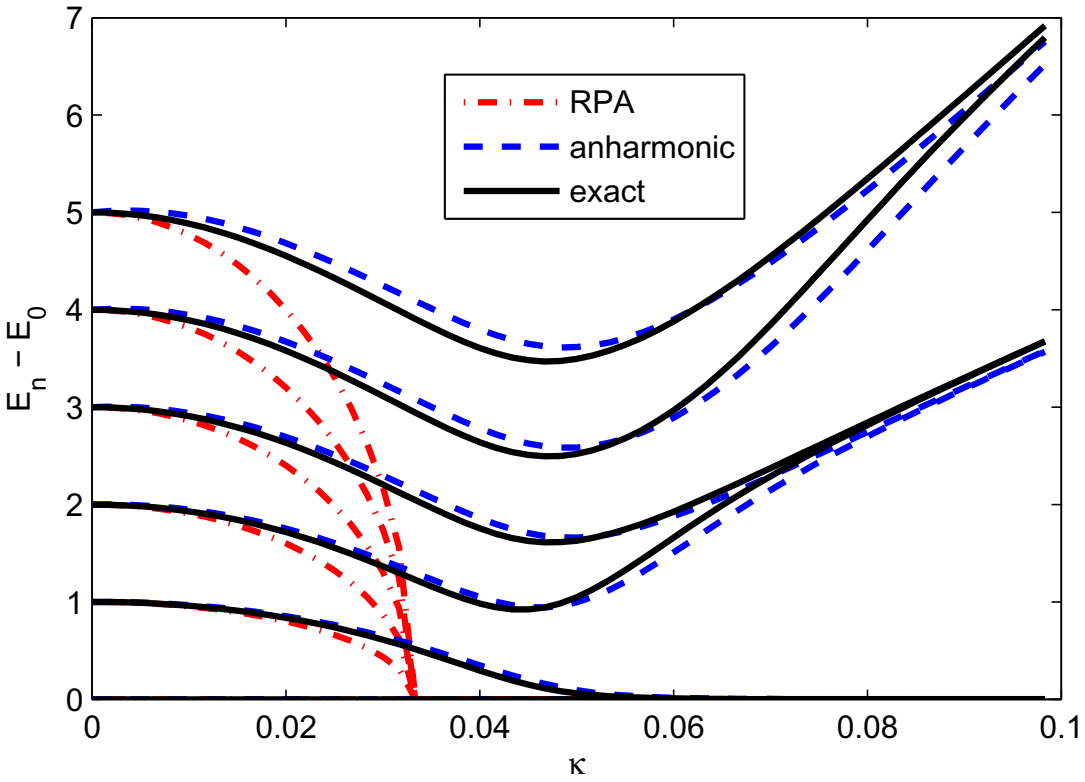

Figure 3.1: The excitation energies $E_n - E_0$ of the first five excited states as a function of κ in the model (3.1) with $\Omega = 30$. The red dashed-dotted line is the RPA calculation (diagonalizing the harmonic Hamiltonian $\frac{\omega^2}{2}\alpha^2 + \frac{1}{2}\pi^2$). The blue dashed line is obtained by diagonalizing $\frac{\omega^2}{2}\alpha^2 + \frac{1}{2}\pi^2 + \frac{\Lambda^{(40)}}{4!}\alpha^4$ in the infinite phonon space $\{|0 \leq n < +\infty\rangle\}$, where ω^2 and $\Lambda^{(40)}$ are given by Eq. (3.10). The black solid line shows the exact results from diagonalizing the original fermionic Hamiltonian (3.1) directly. For interpretation of the references to color in this and all other figures, the reader is referred to the electronic version of this dissertation.

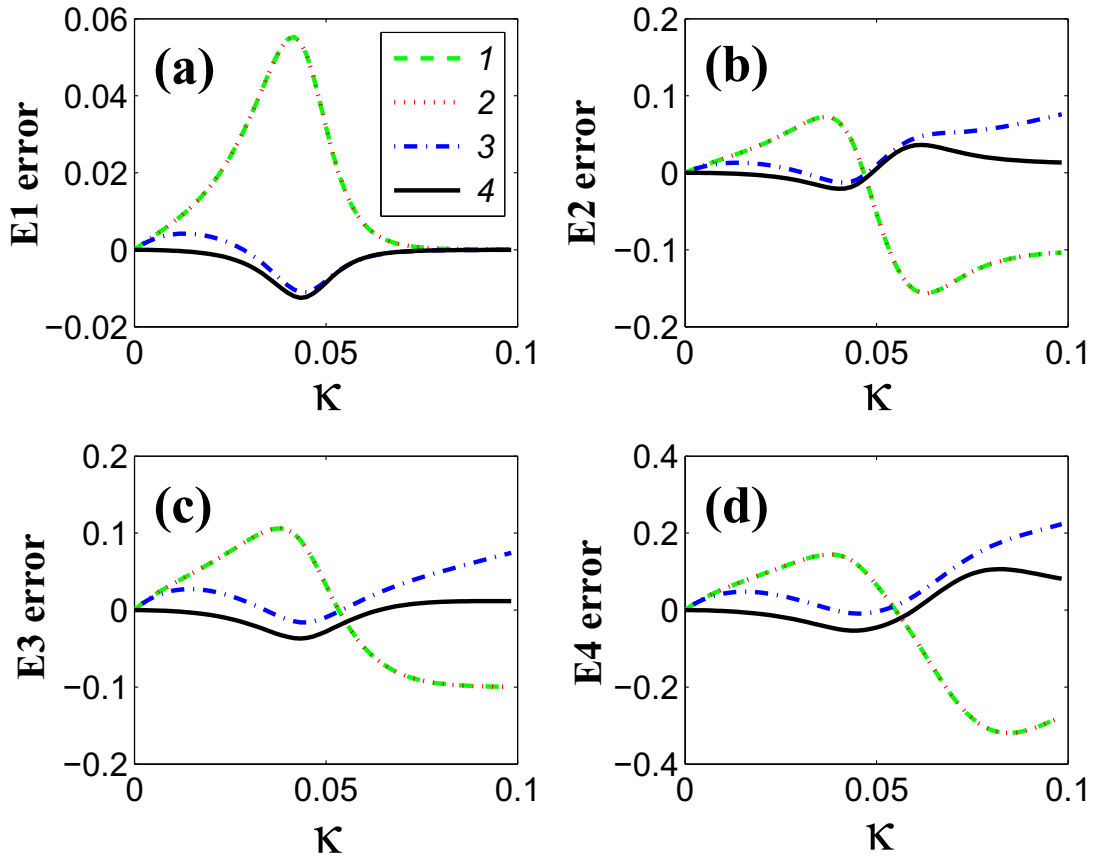

Figure 3.2: The errors of the first four excitation energies $E - E_{\text{exact}}$ as a function of κ in a set of calculations. Panels (a), (b), (c), and (d) are for the first, second, third, and fourth excitation energy, respectively. Four lines on each panel are obtained by diagonalizing different collective Hamiltonians in different phonon spaces. *1* (green dashed line): $H = \frac{\omega^2}{2}\alpha^2 + \frac{1}{2}\pi^2 + \frac{\Lambda^{(40)}}{4!}\alpha^4$ in $\{|0 \le n < +\infty\rangle\}$. *2* (red dotted line): $H = \frac{\omega^2}{2}\alpha^2 + \frac{1}{2}\pi^2 + \frac{\Lambda^{(40)}}{4!}\alpha^4$ in $\{|0 \le n \le \Omega\rangle\}$. *3* (blue dashed-dotted line): $H = \frac{\omega^2}{2}\alpha^2 + \frac{1}{2}\pi^2 + \frac{\Lambda^{(40)}}{4!}\alpha^4$ in $\{|0 \le n \le \Omega\rangle\}$, but with $\omega^2 = 1 - \kappa^2\Omega(\Omega+2)$ replacing that in Eq. (3.10). *4* (black solid line): $H = \frac{\omega^2}{2}\alpha^2 + \frac{1}{2}\pi^2 + \frac{\Lambda^{(40)}}{4!}\alpha^4 + \frac{\Lambda^{(04)}}{4!}\pi^4$ in $\{|0 \le n \le \Omega\rangle\}$, also with $\omega^2 = 1 - \kappa^2\Omega(\Omega+2)$. *1* and *2* closely overlap and are indistinguishable in the figure.

mapped onto the bosonic state $|n=0\rangle$. The result is

$$u^4 = \frac{\sum_{2<F<1} |r_{12}^{(10)}|^2}{\sum_{2<F<1} |r_{12}^{(01)}|^2} \tag{3.11}$$

where the summation indices 1 and 2 run over unoccupied and occupied single-particle levels, respectively ("F" means Fermi surface). In the Lipkin model Eq. (3.11) reproduces the exact result Eq. (3.6). Within the finite physical space, the $\Lambda^{(04)} < 0$ term does not generate divergences and should be kept. In order to identify the errors of the "anharmonic" curve in Fig. 3.1, we plot the errors of the excitation energies for the first four excited states in a set of calculations in Fig. 3.2. The overlap of curves *1* and *2* means that convergence is reached for the first few excitation energies in the finite physical space $\{|0 \leq n \leq \Omega\rangle\}$. Going from curve *2* to curve *3*, we remove the error owing to the inaccuracy of the harmonic potential ω^2 in the next-to-leading order in $1/\Omega$: We replace ω^2 in Eq. (3.10) by $\omega^2 = 1-\kappa^2\Omega(\Omega+2)$, which is correct not only in the leading order but also in the next-to-leading order of $1/\Omega$. Finally in curve *4* the "divergent" term $\Lambda^{(04)} < 0$ is included. We see that *4* is a much better calculation than *1*. The little "kink" on curve *4* near $\kappa = 0.05$ coincides with the phase transition of the system, where the spectrum becomes doubly degenerate inside a well-developed (large enough $\omega^2 < 0$) double-well potential (see Fig. 3.1).

In summary, the *microscopically* calculated "divergent" terms should always be kept in the bosonic Hamiltonian when diagonalizing. Within the *finite* physical space, they mix nearby states without causing divergences. The low-lying collective states should compose mainly of the states with the smallest phonon numbers, therefore be insensitive to small variations (u in Eq. (3.11) and the boundary $n \leq \Omega$) of the physical phonon space. This is the case in models of this thesis.

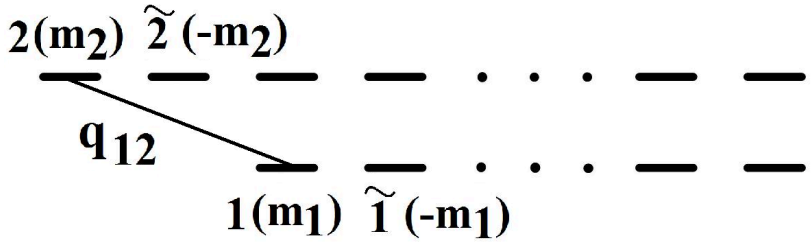

Figure 3.3: Single-particle level scheme. $\tilde{1}$ is the time-reversal level of 1. Each level has a quantum number m.

From Fig. 3.2 we see that the next-to-leading order terms in $1/\Omega$ of the RPA frequency ω^2 could be important. This is the case also in models of the next section. In realistic nuclei, the critical point $\omega^2 \approx 0$ could be reached at a relatively small Ω. For example, $^{100}_{46}$Pd at the critical point [18] has only eight valence particles (although pairing increase collectivity). Hence an achieved improvement would be calculating ω^2 in its next-to-leading order of $1/\Omega$.

3.2 Models with Factorizable Force

In this section we consider models with the factorizable force that resemble the widely used quadrupole-plus-pairing model for realistic nuclei. The single-particle space is drawn schematically in Fig. 3.3. There are two groups of degenerate single-particle levels. The Fermi surface is in between, thus without interaction the lower levels are completely filled and upper levels are empty. Each single-particle level has a quantum number m that is a half-integer. Degenerate time-reversal pairs have m of opposite sign, $m_{\tilde{1}} = -m_1$. For fermions, $|\tilde{\tilde{1}}\rangle = -|1\rangle$, and we choose the phases such that

$$|\widetilde{m}\rangle = |-m\rangle \quad , \quad |\widetilde{-m}\rangle = -|m\rangle \qquad (m > 0).$$

The microscopic fermionic Hamiltonian (2.1) is given in normal-ordering form,

$$H = \sum_1 e_1 a_1^\dagger a_1 + \frac{1}{4} \sum_{1234} V_{1234} N[a_1^\dagger a_2^\dagger a_3 a_4],$$

where $N[a_1^\dagger a_2^\dagger a_3 a_4]$ is the normal-ordering form of operators with respect to the HF ground state. The single-particle energies $e_1 = \pm 1/2$ for the upper and lower levels, respectively. The density matrix without interaction is $\rho_{12} = \delta_{12} n_1$, where the occupation number $n_1 = 1(0)$ for the lower(upper) single-particle levels. The residual interaction is of multipole-multipole type (factorizable),

$$V_{1234} = -\kappa(q_{14} q_{23} - q_{13} q_{24}),$$

where the multipole operator $Q = \sum_{12} q_{12} a_1^\dagger a_2$ is Hermitian and time-even. For simplicity we assume that q is real, thus

$$q_{12} = q_{21} = q_{\tilde{2}\tilde{1}} = q_{\tilde{1}\tilde{2}}.$$

Operator q has certain selection rules with respect to the quantum number m, which will be specified later. We further set diagonal matrix elements of q to zero, $q_{11} = 0$; hence in the mean field, $Q^{(00)} = \mathrm{Tr}[q\rho] = 0$.

In the following we consider four models with different structures (different configurations of single-particle levels and different selection rules of q).

Model 1. We start with the simplest case. Both the upper and lower group have 12 degenerate single-particle levels with quantum numbers $m = \pm\frac{1}{2}, \pm\frac{3}{2}, ..., \pm\frac{11}{2}$. Operator q has the selection rule $\Delta m = 0$, i.e., q_{12} vanishes unless $m_1 = m_2$. The non-vanishing matrix elements q_{12} ($m_1 = m_2$) are set to be 1.

In this model we find by numerical computation an additional "symmetry", namely,

in the Hamiltonian (2.4) there are only three non-vanishing terms : ω^2, $\Lambda^{(40)}$, and $\Lambda^{(22)}$ (besides $\pi^2/2$). This is similar to the "quasi-angular-momentum symmetry" in the Lipkin model, where the only three non-vanishing terms are ω^2, $\Lambda^{(40)}$, and $\Lambda^{(04)}$ (see Sec. 3.1).

The results for this model are shown in Fig. 3.4. The GDM calculation reproduces the exact results of the shell model quite well, both for energies and transition rates. In the shell model we calculated the lowest several states by the Lanczos method. The dashed line in the upper panel is the beginning of the single-particle continuum (single-particle excitations with high level density), only those collective states below the continuum were calculated (due to computation time). In the GDM calculation the resulting bosonic Hamiltonian is diagonalized in the finite "physical" bosonic space $\{|0 \leq n \leq 12\rangle\}$ (12 is the number of fermions). The coefficient u in Eq. (3.5) is fixed by Eq. (3.11). In models of this section, u is a number close to 1. The shown GDM energies and transitions are practically independent of small variations of u around the above value.

As κ increases, the system goes from vibrational to γ-unstable region. In the vibrational region, higher excited states are influenced more by the anharmonicities, as expected. At large κ the spectrum becomes doubly degenerate in a deep double-well potential (large negative ω^2). This is the analog of γ-instability of realistic nuclei in three dimensions.

An important point is that the GDM method works better with increasing collectivity Ω, the number of effective particle-hole excitations contributing to the collective mode. Another calculation has been done (not shown here) with 8 particles in 16 single-particle levels. The GDM results of the current calculation (12 particles in 24 single-particle levels) have very clear improvement over that of the former. In other words, the error in Fig. 3.4 may be of order $1/\Omega$. The largest part of this error may come from the RPA frequency ω^2. At the

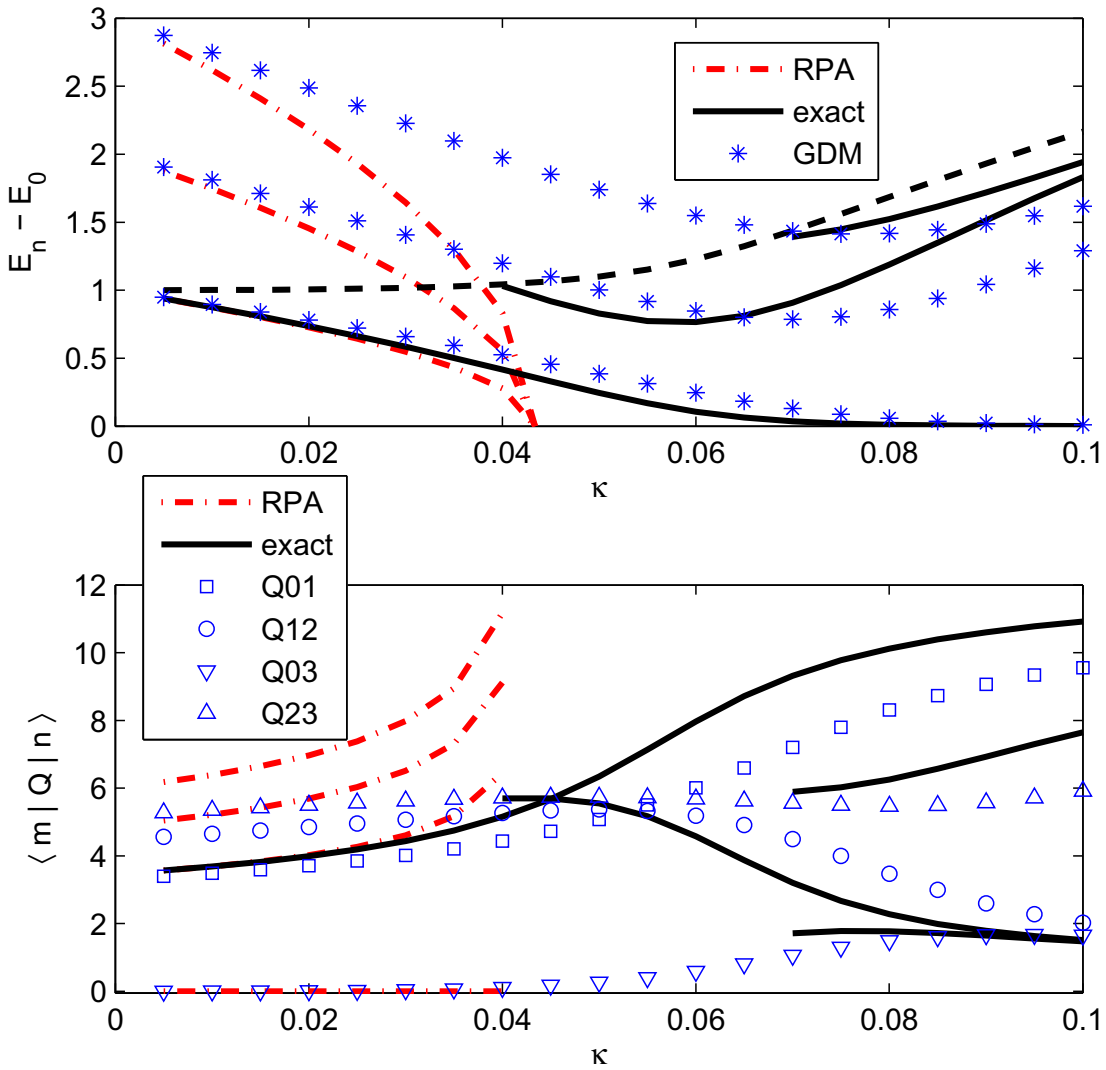

Figure 3.4: Excitation energies $E_n - E_0$ and transition matrix elements $\langle m|Q|n\rangle$ in model 1 as a function of κ. The black solid lines are exact results of shell-model diagonalization. The black dashed line is the beginning of the single-particle continuum. The red dashed-dotted lines are the RPA results. The blue symbols are the GDM results. The stars are energies; the squares, circles, up-triangles and down-triangles are matrix elements of Q between different states. $\langle m|Q|n\rangle$ that are not shown vanish in both the shell model and the GDM calculations.

current stage, the GDM method calculates all $\Lambda^{(mn)}$ in their leading order of $1/\Omega$ but not the next. If the correct $\omega^2 = \Lambda^{(20)}$ was smaller by a $1/\Omega$ term than the one determined here by the RPA equation, all the GDM curves would be shifted to the left (smaller κ), which would decrease greatly the systematic error (see Fig. 3.4). This systematic error owing to inaccurate ω^2 was present in all models in this work (see Figs. 3.5-3.7); Also, it is confirmed in the Lipkin model where everything is known analytically (see Sec. 3.1). Hence an achieved improvement would be calculating ω^2 in its next-to-leading order of $1/\Omega$.

Model 2. This model has the same single-particle configuration but the operator q has now the selection rule $\Delta m = 0, \pm 1$. Non-vanishing q_{12} are still set to be 1. Here we do not find a additional symmetry as in model 1, so the problem exists of what should be the "best" mapping. In the following we did three sets of GDM calculations. The first calculation is possibly the simplest, which keeps only $\Lambda^{(40)}$ (besides $\omega^2\alpha^2/2$ and $\pi^2/2$) in H_b, fixed by the constraint from the 4th order in the equation of motion. The second calculation keeps the lowest two potential (no π dependence) terms $\Lambda^{(40)}$ and $\Lambda^{(60)}$, which are fixed by the two constraints from up to the 6th order in the equation of motion. The third calculation keeps all quartic anharmonicities, $\Lambda^{(40)}$, $\Lambda^{(22)}$, and $\Lambda^{(04)}$, fixed by the three constraints from up to the 8th order in the equation of motion.

We first notice in Fig. 3.5 that in this model the single-particle continuum goes down with increasing κ, as opposed to going up in model 1. This is because now mixing of single-particle levels within the upper(lower) group is allowed by the selection rule that Δm can be ± 1. As a result, originally degenerate levels from the upper(lower) group get a finite spread, which reduces the gap of the single-particle continuum. Only the first excited state is within the gap and calculated in the shell model.

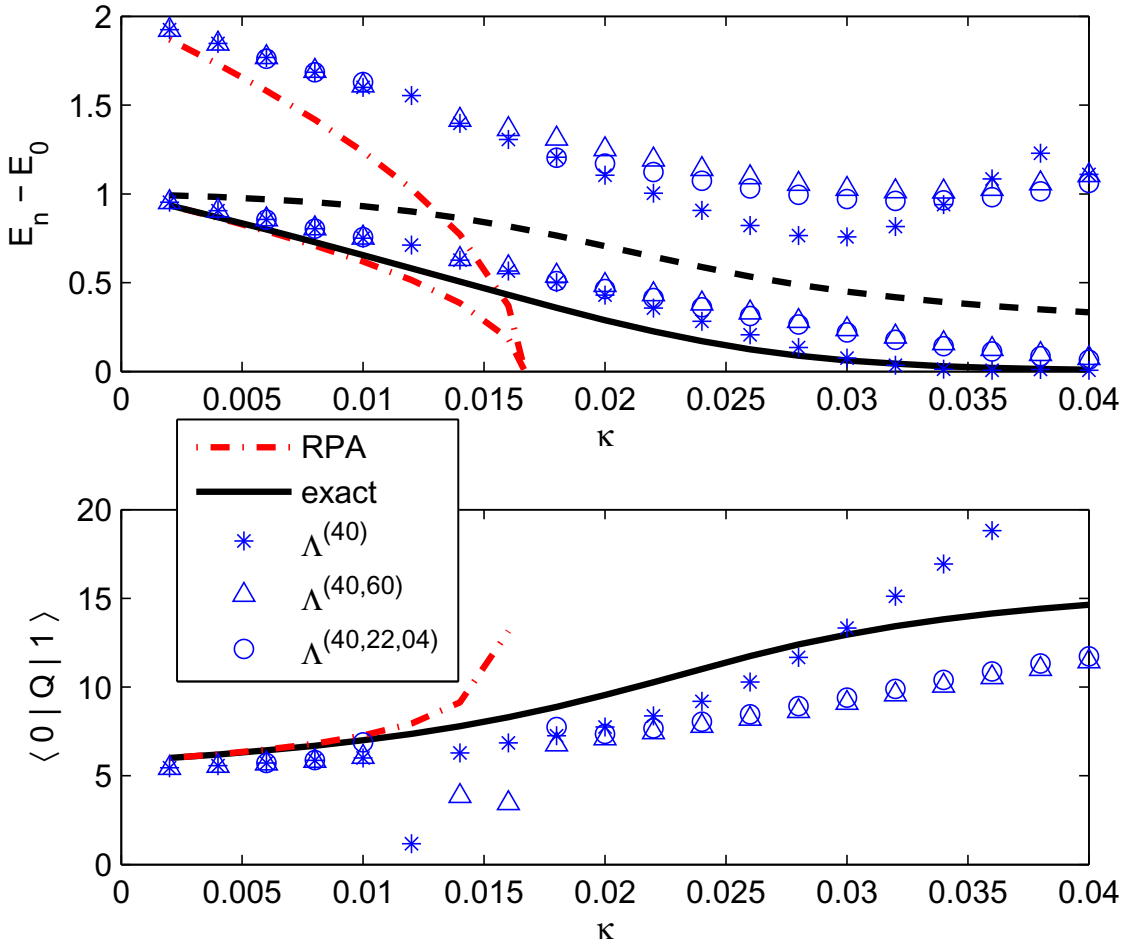

Figure 3.5: Excitation energies $E_n - E_0$ and transition matrix elements $\langle 0|Q|1\rangle$ in model 2 as a function of κ. The black solid lines are exact results of shell-model diagonalization. The black dashed line is the beginning of the single-particle continuum. The red dashed-dotted lines are the RPA results. The blue symbols (stars, up-triangles and circles) are results of three different sets of GDM calculations, as labeled in the legend.

In the GDM calculations we see that the simplest one degree-of-freedom ($\Lambda^{(40)}$) calculation is reasonably well in most cases except at very large κ. The other two calculations ($\Lambda^{(40/60)}$ and $\Lambda^{(40/22/04)}$) give essentially the same results (for the quantities shown in Fig. 3.5), although their common parameter, $\Lambda^{(40)}$, is different. This insensitivity of GDM results to the degrees of freedom chosen, is important. As we said in Sec. 2.6, two different bosonic Hamiltonians could be equivalent if they were related by canonical transformations/renormalizations (2.34) of variables α and π. This insensitivity simply says that the GDM formalism knows these renormalizations and does them correctly. In model 1 we also find this insensitivity (not shown). Finally we notice that in regions of $\omega^2 \sim 1/\Omega$, calculations that go to higher orders in the equation of motion may give unphysical results. This is again because the equation of motion are accurate only in the leading order of $1/\Omega$. The fact that this "divergence" appears slightly before the instability point of RPA shown in Fig. 3.5, indicates again that the correct ω^2 may be smaller than the one calculated by RPA.

Models 3 and 4. At last we consider two models with single-particle configurations that are asymmetric in upper and lower groups, which generates odd anharmonicities that are necessary for deformation. In model 3, the lower group has 10 single-particle levels with $m = \pm\frac{3}{2}, ..., \pm\frac{11}{2}$, the upper group has 14 single-particle levels with $m = \pm\frac{1}{2}, ..., \pm\frac{13}{2}$. In model 4, the lower group has 12 single-particle levels with $m = \pm\frac{1}{2}, ..., \pm\frac{11}{2}$, the upper group has 10 single-particle levels with $m = \pm\frac{1}{2}, ..., \pm\frac{9}{2}$. In both models, operator q still has the selection rule of $\Delta m = 0, \pm 1$, with non-vanishing matrix elements set to be 1. Model 3 has a slightly larger asymmetry than that of model 4, and their signs of the asymmetry are different.

These two models are more complicated in the sense that now there are more active

degrees of freedom (odd anharmonicities). In the GDM method, we do a possibly simplest calculation. We keep in H_b only $\Lambda^{(30)}$, $\Lambda^{(12)}$, and $\Lambda^{(40)}$ (besides $\omega^2\alpha^2/2$ and $\pi^2/2$). $\Lambda^{(30)}$ and $\Lambda^{(12)}$ are fixed by requiring $Q^{(20)} = Q^{(02)} = 0$ in the solution (2.40). Then $\Lambda^{(40)}$ is fixed by the constraint from the 4th order in the equation of motion. The requirement $Q^{(20)} = Q^{(02)} = 0$ is the same as that for models 1 and 2 without upper-lower asymmetry, by which $\Lambda^{(30)}$ and $\Lambda^{(12)}$ vanish.

The results are shown in Figs. 3.6-3.7. The deformation begins around the critical point of RPA when ω^2 becomes negative. In the vibrational region the potential is stiff and deformation is not easy. As κ increases, the potential becomes flat in bottom and finally of a double-well shape. Then, even a relatively small odd anharmonicity (here mainly $\Lambda^{(30)}$) can tilt the potential and generate large deformation. We notice firstly that the GDM calculations give the correct sign of deformations: positive/negative for the ground/first-excited state of model 3, and vice versa for model 4. In the realistic situation of three dimensions, $\Lambda^{(30)}((\hat{\alpha} \times \hat{\alpha})^2 \times \hat{\alpha})^0 \sim \Lambda^{(30)}\beta^3 \cos 3\gamma$ ($\hat{\alpha}$ is the quadrupole phonon and β, γ are Bohr shape variables), the sign of $\Lambda^{(30)}$ "determines" the intrinsic shape of the nucleus (prolate or oblate). This is especially interesting in the transitional regions where the rotor formula is not applicable. Secondly, the quantitative agreement of deformation is also good except at the largest κ. There the deformation "saturates" towards its maximal possible value within the model space, favored by energy. Meanwhile in the boson mapping, we are too close to the boundary of the finite physical bosonic space, and the GDM results become inaccurate. In realistic nuclei this "saturation" may not happen. The number of participating/active nucleons is usually around 30 in well-deformed nuclei, which is much larger than that around 10 in the current models. Finally, we would like to point out that the first excited state in

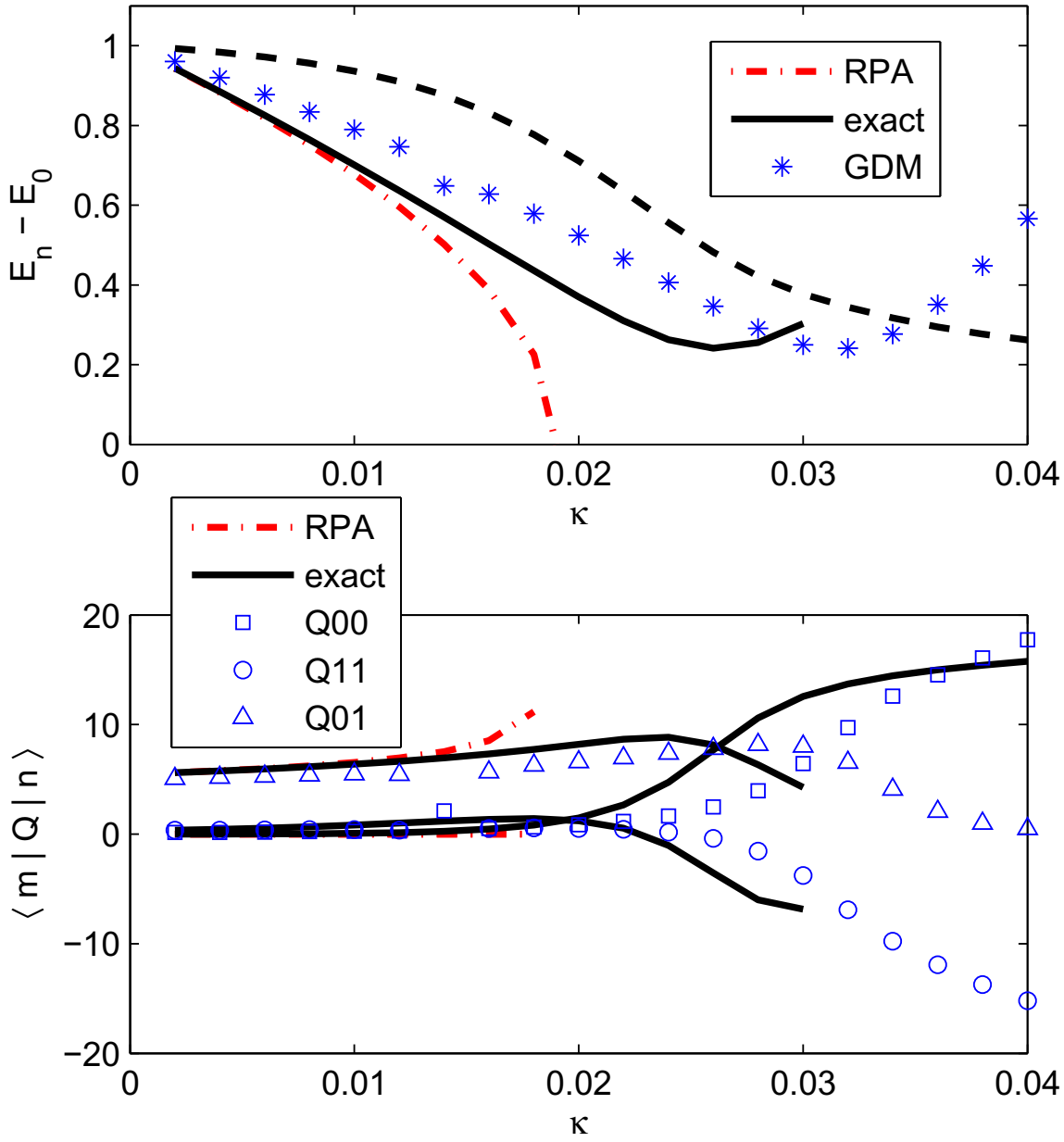

Figure 3.6: Excitation energies $E_n - E_0$ and transition matrix elements $\langle m|Q|n\rangle$ in model 3 as a function of κ. The black solid lines are exact results of shell-model diagonalization. The black dashed line is the beginning of the single-particle continuum. The red dashed-dotted lines are the RPA results. The blue symbols are the GDM results. The stars are energies; the squares, circles and up-triangles are matrix elements of Q between different states.

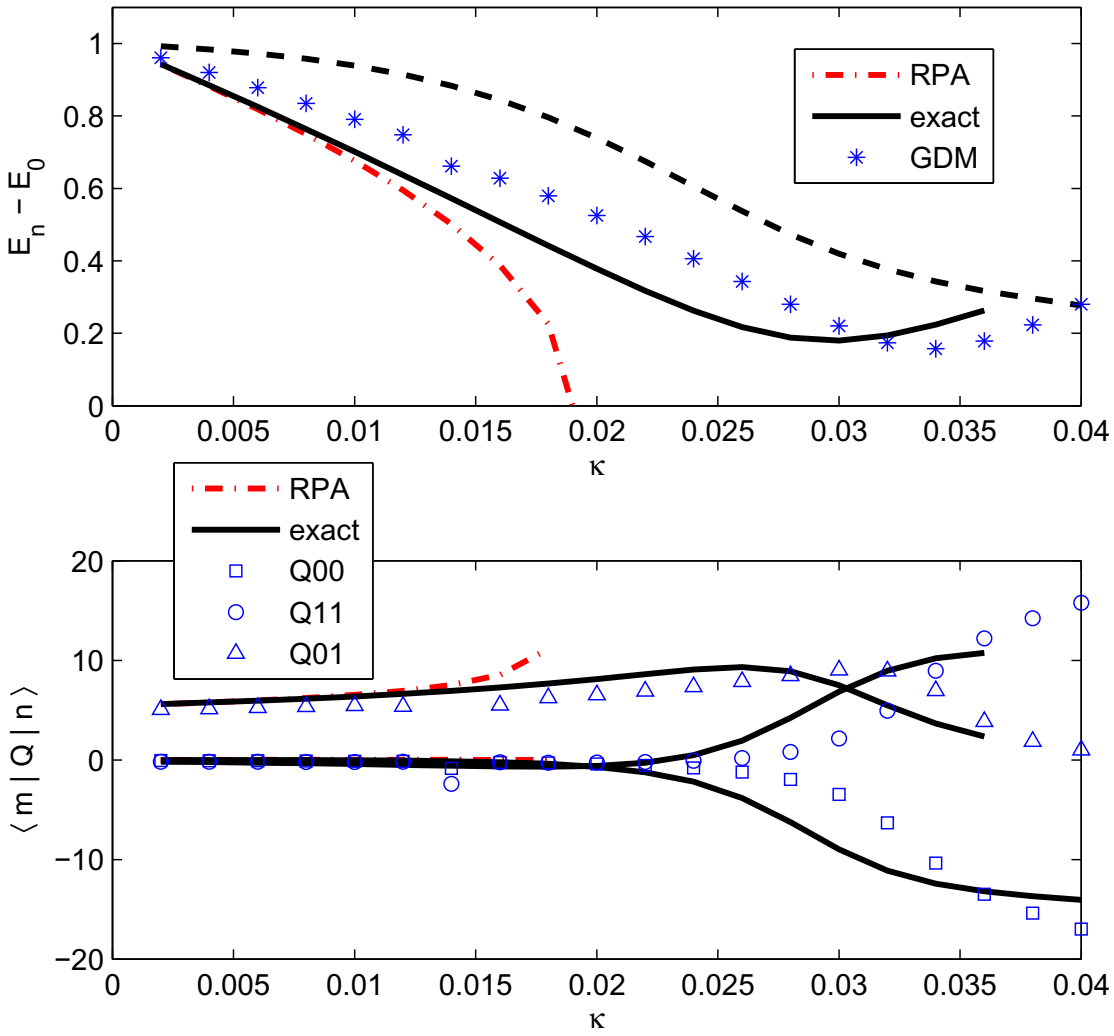

Figure 3.7: Excitation energies $E_n - E_0$ and transition matrix elements $\langle m|Q|n\rangle$ in model 4 as a function of κ. The black solid lines are exact results of shell-model diagonalization. The black dashed line is the beginning of the single-particle continuum. The red dashed-dotted lines are the RPA results. The blue symbols are the GDM results. The stars are energies; the squares, circles and up-triangles are matrix elements of Q between different states.

our simple models is not a "rotational" state, rather it corresponds to the next "band head" in realistic rotational nuclei. The rotational states that are very low in energy come in only in three dimensions.

To summarize, in this chapter we demonstrate the validity of the GDM procedure for microscopic calculation of the collective/bosonic Hamiltonian. The lowest several states of this bosonic Hamiltonian quite well reproduce the collective states of the exact shell model, both for energies and transition rates, in a wide range from vibrational, γ-unstable, to deformed systems. Specifically, we show that deformation can be described without introducing a deformed mean field. The traditional procedure of "symmetry breaking and restoration", first "statically" breaks rotational symmetry in the ground state, by representing the latter as a Slater determinant of deformed single-particle levels (Nilsson levels); then projects afterwards to good angular momentum. However, in case of large shape fluctuations (flat minimum of energy surface) or shape coexistence (two close minima), it may fail. On the other hand, the GDM procedure always conserves the rotational symmetry. Deformations are put in "dynamically" at higher orders (for example cubic terms) beyond the mean field. Thus it is suitable to describe such phenomena as shape fluctuations and coexistence.

In realistic nuclei, the gap of the single-particle continuum is generated by pairing correlations. The GDM formalism based on the Hartree-Fock-Bogoliubov variational method is straightforward as will be shown in the following chapters. However, another treatment may be possible. Instead of introducing Bogoliubov quasi-particles and representing the ground state as their vacuum, the pairing correlations are considered in higher orders beyond the mean field, by keeping both the particle-hole and particle-particle channels in the factoriza-

tion $a_4^\dagger a_3^\dagger a_2 a_1 \approx a_4^\dagger a_1 \cdot a_3^\dagger a_2 - a_4^\dagger a_2 \cdot a_3^\dagger a_1 + a_4^\dagger a_3^\dagger \cdot a_2 a_1$. In this way the exact particle number is always conserved. Work along this line is in progress and results seem promising.

Chapter 4

Formalism for Realistic Nuclei

In this chapter we consider the GDM formalism for realistic nuclei. There are three complications. A realistic nucleus has two kinds of fermions; symmetries, e.g. rotational invariance, need to be respected; and pairing correlations should be considered.

As in the BCS theory we substitute the original system by a grand-canonical ensemble, in which the chemical potential is fixed by the average particle number of the ground state in the mean-field order. In this case we need to consider the equation of motion of not only $a_2^\dagger a_1$ but also $a_2 a_1$. A good treatment of the superfluid ground state, on top of which collective excitations are formed, is essential.

The collective mode operators $\alpha_{\lambda\mu}$, $\pi_{\lambda\mu}$ have quantum numbers (angular momentum λ and its projection μ) corresponding to symmetries of the Hamiltonian. In this section we keep only the quadrupole mode ($\lambda = 2$) which is the most important one at low energy. The case of interacting modes (quadrupole and octupole) is discussed briefly in Appendix D.

4.1 Formalism

The microscopic fermionic Hamiltonian for the grand-canonical ensemble is still given by Eq. (2.1): we include the $-\mu\hat{N}$ term in $\hat{\epsilon}$ (μ is the chemical potential and $\hat{N}$ is the particle number operator), and the single-particle index 1, 2 ... can run over protons and neutrons. Isospin may not be conserved for some effective interactions. We do not write V in the form $V^J_{(j_1 j_2),(j_3 j_4)}$; ϵ_{12} and V_{1234} carry all the symmetries of H implicitly.

Now the reference state $|\Phi\rangle$ does not have definite particle number,

$$\langle\Phi|a_1^\dagger a_2|\Phi\rangle \equiv \rho_{21}, \quad \langle\Phi|a_1 a_2|\Phi\rangle \equiv \kappa_{21}, \tag{4.1}$$

where κ is the pair correlator [19]. And we need two density matrix operators

$$R_{12} \equiv a_2^\dagger a_1, \quad K_{12} \equiv a_2 a_1, \tag{4.2}$$

and two self-consistent field operators

$$W\{R\}_{12} \equiv \sum_{34} V_{1432} R_{34}, \quad f\{R\} \equiv \epsilon + W\{R\}, \tag{4.3}$$

$$\Delta\{K\}_{12} \equiv \frac{1}{2}\sum_{34} V_{1234} K_{43}. \tag{4.4}$$

It will be convenient to introduce (R^T, f^T are transposed matrices)

$$D\{R,K\} \equiv \begin{pmatrix} R & K \\ K^\dagger & I - R^T \end{pmatrix} \quad , \quad S\{R,K\} \equiv \begin{pmatrix} f\{R\} & \Delta\{K\} \\ \Delta^\dagger\{K\} & -f^T\{R\} \end{pmatrix}. \tag{4.5}$$

The expansion of density matrix operators replacing Eq. (2.12) is now over the multipole

mode operators $\alpha_{\lambda\mu}$ and $\pi_{\lambda\mu}$. The operator structures are more complicated owing to angular-momentum vector coupling. Let us choose the basis for the expansion as $\{O_\chi\}$, where χ combines all the necessary quantum numbers to specify a term in the basis, including the power of coordinate a (α^a), the power of momentum b (π^b), the total angular momentum L, and others. For example, $O_\chi = \{(\alpha \times \alpha)^l, \pi\}^L$ has χ as a summary of $a = 2$, $b = 1$, L, l. Hence the expansions of R, K replacing Eq. (2.12) are

$$R = \sum_\chi [r_\chi O_\chi]^0_0, \quad K = \sum_\chi [k_\chi O_\chi]^0_0, \tag{4.6}$$

where r_χ, k_χ are matrices in the single-particle space. The symbol $[\ ]^0_0$ means angular-momentum vector coupling to a scalar. Substituting Eq. (4.6) into Eq. (4.5) we get the expansion of the latter

$$D = \sum_\chi [D_\chi O_\chi]^0_0, \quad S = \sum_\chi [S_\chi O_\chi]^0_0, \tag{4.7}$$

where D_χ and S_χ have a dimension that is twice of that of r_χ and k_χ.

Similarly, in the expansion of the Hamiltonian only the scalar terms ($L = 0$) exist. We choose the basis as $\{O_\beta\}$. In principle the choice of β can be different from χ. The expansion of H replacing Eq. (2.11) is

$$H = \sum_\beta \Lambda_\beta O_\beta \tag{4.8}$$

In addition to Eq. (2.7), we calculate the exact equation of motion $[K_{12}, H]$. On the

right-hand side of the resulting equations, we substitute the factorization

$$a_4^\dagger a_3^\dagger a_2 a_1 \doteq a_4^\dagger a_1 \cdot a_3^\dagger a_2 - a_4^\dagger a_2 \cdot a_3^\dagger a_1 + a_4^\dagger a_3^\dagger \cdot a_2 a_1 \tag{4.9}$$

replacing Eq. (2.8). In Eq. (4.9) both the particle-particle and particle-hole channels are kept. The results can be summarized as

$$[D, H] \doteq [S, D]. \tag{4.10}$$

This is the equation of motion in the collective band replacing Eq. (2.9).

Let us introduce the group algebraic properties

$$[O_\chi, O_\beta] = i \sum_\lambda \langle \chi\beta \| \lambda \rangle O_\lambda, \tag{4.11}$$

where $\langle \chi\beta \| \lambda \rangle$ vanishes unless $L_\lambda = L_\chi$, $a_\lambda = a_\chi + a_\beta - 1$, $b_\lambda = b_\chi + b_\beta - 1$. And

$$(O_\chi O_\eta)^L = \sum_\lambda^{L_\lambda = L} \langle (\chi\eta) \| \lambda \rangle O_\lambda, \tag{4.12}$$

where $\langle (\chi\eta) \| \lambda \rangle$ vanishes unless $a_\lambda = a_\chi + a_\eta$, $b_\lambda = b_\chi + b_\eta$. $\langle \chi\beta \| \lambda \rangle$ and $\langle (\chi\eta) \| \lambda \rangle$ are complicated basis-dependent (χ and β) expressions consisting of Clebsch-Gordan coefficients. Substituting Eqs. (4.11) and (4.12) into Eq. (4.10) we get

$$i \sum_\chi \sum_\beta \sum_\lambda \Lambda_\beta \langle \chi\beta \| \lambda \rangle [D_\chi O_\lambda]_0^0$$
$$= \sum_\chi \sum_\eta \sum_\lambda \langle (\chi\eta) \| \lambda \rangle \langle [(L_\chi L_\chi) 0 (L_\eta L_\eta) 0] 0 | [(L_\chi L_\eta) L_\lambda (L_\chi L_\eta) L_\lambda] 0 \rangle \ [[S_\chi, D_\eta]^{L_\lambda} O_\lambda]_0^0.$$

On the right-hand side, $\langle[(L_\chi L_\chi)0(L_\eta L_\eta)0]0|[(L_\chi L_\eta)L_\lambda(L_\chi L_\eta)L_\lambda]0\rangle$ is a $9j$-symbol. Since terms O_λ in the basis are linearly independent, we get one equation for each O_λ equating the corresponding coefficients,

$$i\sum_\chi\sum_\beta \Lambda_\beta\langle\chi\beta\|\lambda\rangle D_\chi$$
$$= \sum_\chi\sum_\eta\langle(\chi\eta)\|\lambda\rangle\langle[(L_\chi L_\chi)0(L_\eta L_\eta)0]0|[(L_\chi L_\eta)L_\lambda(L_\chi L_\eta)L_\lambda]0\rangle\ [S_\chi, D_\eta]^{L_\lambda}. \qquad (4.13)$$

This is the final set of GDM equations replacing Eq. (2.14). The "kinematic" coefficients for rotational symmetry are singled out. The "dynamics" from the Hamiltonian is hidden in the self-consistent field S_χ (4.5). Equation (4.13) is valid for the general case of interacting multiple collective modes (for an example see appendix D). In the next section we list explicitly its lowest orders in the case of a single quadrupole mode.

4.2 Equations of Motion for Quadrupole Phonon

The multipole mode operators $\alpha^\dagger_{\lambda\mu}$, $\pi^\dagger_{\lambda\mu}$ carry quantum numbers of angular momentum λ, its projection μ, and parity $(-)^\lambda$. The coordinate $\alpha^\dagger_{\lambda\mu}$ is time-even, and the momentum $\pi^\dagger_{\lambda\mu}$ is time-odd. Their Hermitian properties are

$$\alpha^\dagger_{\lambda\mu} = (-)^{\lambda-\mu}\alpha_{\lambda-\mu}, \quad \pi^\dagger_{\lambda\mu} = (-)^{\lambda-\mu}\pi_{\lambda-\mu}. \qquad (4.14)$$

The commutation relation is given by

$$[\alpha^\dagger_{\lambda\mu}, \pi_{\lambda'\mu'}] = i\ \delta_{\lambda\lambda'}\delta_{\mu\mu'}. \qquad (4.15)$$

Here we consider only the quadrupole mode $\lambda = 2$, and drop the label λ.

The basis $\{O_\chi\}$ is specified in the following expansion of the density matrix operators,

$$\begin{aligned} R = \rho + \sum_\mu r^{(10)}_\mu \alpha^\dagger_\mu + \sum_\mu r^{(01)}_\mu \pi^\dagger_\mu + \frac{1}{2}\sum_{L=0,2,4}\sum_\mu r^{(20)}_{L\mu}(\alpha^\dagger \times \alpha^\dagger)^L_\mu \\ + \frac{1}{2}\sum_{L=0,2,4}\sum_\mu r^{(02)}_{L\mu}(\pi^\dagger \times \pi^\dagger)^L_\mu + \frac{1}{2}\sum_{L=0,1,2,3,4}\sum_\mu r^{(11)}_{L\mu}\{\alpha^\dagger, \pi^\dagger\}^L_\mu \\ + \frac{1}{6}\sum_{L=0,2,3,4,6}\sum_\mu r^{(30)}_{L\mu}\{(\alpha^\dagger \times \alpha^\dagger)^{l_L}, \alpha^\dagger\}^L_\mu + \frac{1}{6}\sum_{L=0,2,3,4,6}\sum_\mu r^{(03)}_{L\mu}\{(\pi^\dagger \times \pi^\dagger)^{l_L}, \pi^\dagger\}^L_\mu \\ + \frac{1}{4}\sum_{L=0,1,2,3,4,5,6}\sum_{l=0,2,4}\sum_\mu r^{(21)}_{Ll\mu}\{(\alpha^\dagger \times \alpha^\dagger)^l, \pi^\dagger\}^L_\mu \\ + \frac{1}{4}\sum_{L=0,1,2,3,4,5,6}\sum_{l=0,2,4}\sum_\mu r^{(12)}_{Ll\mu}\{\alpha^\dagger, (\pi^\dagger \times \pi^\dagger)^l\}^L_\mu + \ldots \end{aligned} \tag{4.16}$$

Three identical d bosons can couple to $L = 0, 2, 3, 4, 6$. In the α^3 and π^3 terms of Eq. (4.16) we choose the intermediate quantum number for each L to be l_L; this choice will not influence the final results. Similarly the expansion for the operator K is

$$K = \kappa + \sum_\mu k^{(10)}_\mu \alpha^\dagger_\mu + \sum_\mu k^{(01)}_\mu \pi^\dagger_\mu + \frac{1}{2}\sum_{L=0,2,4}\sum_\mu k^{(20)}_{L\mu}(\alpha^\dagger \times \alpha^\dagger)^L_\mu + \ldots \tag{4.17}$$

The basis $\{O_\beta\}$ is specified in the expansion of the Hamiltonian,

$$\begin{aligned} H = E_0 + \frac{\omega^2}{2}\sqrt{5}(\alpha \times \alpha)^0_0 + \frac{1}{2}\sqrt{5}(\pi \times \pi)^0_0 \\ + \frac{\Lambda^{(30)}}{6}\sqrt{5}\{(\alpha \times \alpha)^2, \alpha\}^0_0 + \frac{\Lambda^{(12)}}{4}\sqrt{5}\{\alpha, (\pi \times \pi)^2\}^0_0 \\ + \frac{\Lambda^{(40)}}{4}\sqrt{5}((\alpha \times \alpha)^0 \times (\alpha \times \alpha)^0)^0_0 + \frac{\Lambda^{(04)}}{4}\sqrt{5}((\pi \times \pi)^0 \times (\pi \times \pi)^0)^0_0 \\ + \sum_{L=0,2,4}\frac{\Lambda^{(22)}_L}{8}\sqrt{5}\{(\alpha \times \alpha)^L, (\pi \times \pi)^L\}^0_0 + \ldots . \end{aligned} \tag{4.18}$$

H is Hermitian, time-even, invariant under rotation and inversion.

4.2.1 Hartree-Fock-Bogoliubov Equation

In the mean-field order, the constant terms of Eq. (4.13) give the HFB equation,

$$[S^{(00)}, D^{(00)}] = 0. \tag{4.19}$$

Equation (4.19) says that $S^{(00)}$ and $D^{(00)}$ can be diagonalized simultaneously,

$$\left[\begin{pmatrix} E & 0 \\ 0 & -E \end{pmatrix}, \begin{pmatrix} n & 0 \\ 0 & I-n \end{pmatrix} \right] = 0, \tag{4.20}$$

where E and n are diagonal matrices. The chemical potential μ (buried in E) is determined by $N = \mathrm{Tr}\{\rho\} = \sum_1 \rho_{11} = \sum_1 n_1$. We introduce the quasiparticle operators $b_\lambda^\dagger$, b_λ through the unitary canonical transformation

$$b_\lambda = \sum_1 (u_{1\lambda}^* a_1 - v_{1\lambda} a_1^\dagger),\ b_\lambda^\dagger = \sum_1 (u_{1\lambda} a_1^\dagger - v_{1\lambda}^* a_1). \tag{4.21}$$

If the reference state $|\Phi\rangle$ is a "quasiparticle vacuum", $|\Phi\rangle = \mathrm{norm} \cdot \prod_\lambda b_\lambda |0\rangle$, then by Eq. (4.1) we get:

$$\rho = vv^\dagger, \quad \kappa = -vu^T. \tag{4.22}$$

In this case $D^{(00)}$ is diagonalized by the canonical transformation (4.21):

$$U = \begin{pmatrix} u^\dagger & -v^T \\ -v^\dagger & u^T \end{pmatrix}, \quad UD^{(00)}U^\dagger = \begin{pmatrix} 0 & 0 \\ 0 & I \end{pmatrix}, \tag{4.23}$$

where the matrix n in Eq. (4.20) vanishes. The HFB equation (4.19) requires that $S^{(00)}$ be diagonalized by U simultaneously. In this work we assume that $|\Phi\rangle$ is a "quasiparticle vacuum". From now on we always work in the quasiparticle basis (multiplying Eq. (4.13) by U from the left and $U^\dagger$ from the right).

4.2.2 Quasi-Particle Random Phase Approximation

In the harmonic order, the linear terms of Eq. (4.13) give the QRPA equations

$$\underline{\pi^\dagger_\mu}: \qquad iD^{(10)} = [S^{(00)}, D^{(01)}] + [S^{(01)}, D^{(00)}], \tag{4.24}$$

$$\underline{\alpha^\dagger_\mu}: \quad -i\omega^2 D^{(01)} = [S^{(00)}, D^{(10)}] + [S^{(10)}, D^{(00)}]. \tag{4.25}$$

This is a linear homogenous set of equations for $D^{(10)}$ and $D^{(01)}$, a non-zero solution requires a zero determinant, from which we solve for the QRPA frequency ω^2.

4.2.3 Cubic Order

In the cubic order, Eq. (4.13) gives

$$\underline{(\alpha^\dagger \times \alpha^\dagger)^L_\mu/2, L = 0, 2, 4:}$$

$$-2i\omega^2 D^{(11)}_L - 2i\delta_{L,2}\Lambda^{(30)}D^{(01)} = [S^{(00)}, D^{(20)}_L] + [S^{(20)}_L, D^{(00)}] + 2\,[S^{(10)}, D^{(10)}]^L, \tag{4.26}$$

$$\underline{(\pi^\dagger \times \pi^\dagger)^L_\mu/2, L=0,2,4:}$$

$$2iD^{(11)}_L - i\delta_{L,2}\Lambda^{(12)}D^{(01)} = [S^{(00)}, D^{(02)}_L] + [S^{(02)}_L, D^{(00)}] + 2\ [S^{(01)}, D^{(01)}]^L, \tag{4.27}$$

$$\underline{\{\alpha^\dagger, \pi^\dagger\}^L_\mu/2, L=0,1,2,3,4:}$$

$$\begin{aligned} &-i\delta_{L,\mathrm{even}}\omega^2 D^{(02)}_L + i\delta_{L,\mathrm{even}}D^{(20)}_L + i\delta_{L,2}\Lambda^{(12)}D^{(10)} \\ &= [S^{(00)}, D^{(11)}_L] + [S^{(11)}_L, D^{(00)}] + [S^{(10)}, D^{(01)}]^L - [D^{(10)}, S^{(01)}]^L. \end{aligned} \tag{4.28}$$

4.2.4 Quartic Order

In the quartic order, Eq. (4.13) gives

$$\underline{\{(\alpha^\dagger \times \alpha^\dagger)^{l_L}, \alpha^\dagger\}^L_\mu/6, L=0,2,3,4,6:}$$

$$\begin{aligned} &-\frac{3i}{2}\omega^2 \sum_{l=0,2,4} D^{(21)}_{Ll}\cdot\gamma^L_{l,l_L} - 3i(-)^L\Lambda^{(30)}D^{(11)}_L\cdot\gamma^L_{2,l_L} - 3i\delta_{L2}\Lambda^{(40)}D^{(01)}\cdot\gamma^{L=2}_{0,l_L} \\ &= [S^{(00)}, D^{(30)}_L] + [S^{(30)}_L, D^{(00)}] + \frac{3}{2}\sum_{l=0,2,4}([S^{(20)}_l, D^{(10)}]^L - [D^{(20)}_l, S^{(10)}]^L)\cdot\gamma^L_{l,l_L}, \end{aligned} \tag{4.29}$$

$$\underline{\{(\alpha^\dagger \times \alpha^\dagger)^l, \pi^\dagger\}^L_\mu/4; l=0,2,4; L=0,1,2,3,4,5,6:}$$

$$\begin{aligned} &-2i(-)^L\omega^2 \sum_{l'=0,2,4} D^{(12)}_{Ll'}\cdot g^L_{l,l'} + \frac{2i}{3}\ \delta_{l,l_L}D^{(30)}_L + \frac{4\ i}{3}D^{(30)}_L\cdot g^L_{l,l_L} \\ &-2i\ \delta_{l2}\ \Lambda^{(30)}D^{(02)}_L + 2\ i\Lambda^{(12)}D^{(20)}_L\cdot g^L_{l,2} + i\ \delta_{L2}\ \Lambda^{(22)}_l D^{(10)} \\ &= [S^{(00)}, D^{(21)}_{Ll}] + [S^{(21)}_{Ll}, D^{(00)}] + [S^{(20)}_l, D^{(01)}]^L - [D^{(20)}_l, S^{(01)}]^L \\ &+2\sum_{l'=0,1,2,3,4}([S^{(11)}_{l'}, D^{(10)}]^L - [D^{(11)}_{l'}, S^{(10)}]^L)\cdot g^L_{l,l'}, \end{aligned} \tag{4.30}$$

$$\underline{\{\alpha^\dagger,(\pi^\dagger\times\pi^\dagger)^l\}^L_\mu/4; l=0,2,4; L=0,1,2,3,4,5,6:}$$

$$-\frac{2i}{3}\delta_{l,l_L}(-)^L\omega^2 D^{(03)}_L-\frac{4i}{3}\omega^2 D^{(03)}_L(-)^{L-l_L}\cdot g^L_{l,l_L}+2i(-)^L\sum_{l'=0,2,4}D^{(21)}_{Ll'}\cdot g^L_{l,l'}$$

$$-i\delta_{l2}\Lambda^{(12)}D^{(11)}_L+2i(-)^L\Lambda^{(12)}D^{(11)}_L\cdot g^L_{l,2}-i\ \delta_{L2}\ \Lambda^{(22)}_l D^{(01)}$$

$$=[S^{(00)},D^{(12)}_{Ll}]+[S^{(12)}_{Ll},D^{(00)}]+[S^{(10)},D^{(02)}_l]^L-[D^{(10)},S^{(02)}_l]^L$$

$$+2\sum_{l'=0,1,2,3,4}([S^{(11)}_{l'},D^{(01)}]^L-[D^{(11)}_{l'},S^{(01)}]^L)(-)^{L-l'}g^L_{l,l'},\qquad(4.31)$$

$$\underline{\{(\pi^\dagger\times\pi^\dagger)^{l_L},\pi^\dagger\}^L_\mu/6, L=0,2,3,4,6:}$$

$$\frac{3i}{2}(-)^L\sum_{l=0,2,4}D^{(12)}_{Ll}\cdot\gamma^L_{l,l_L}-\frac{3i}{2}\Lambda^{(12)}D^{(02)}_L\cdot\gamma^L_{2,l_L}+3i\delta_{L2}\Lambda^{(04)}D^{(10)}\cdot\gamma^{L=2}_{0,l_L}$$

$$=[S^{(00)},D^{(03)}_L]+[S^{(03)}_L,D^{(00)}]+\frac{3}{2}\sum_{l=0,2,4}([S^{(02)}_l,D^{(01)}]^L-[D^{(02)}_l,S^{(01)}]^L)\cdot\gamma^L_{l,l_L}.\quad(4.32)$$

The numerical coefficients $\gamma^L_{l,l'}$ and $g^L_{l,l'}$ are defined by

$$\{(\alpha\times\alpha)^l,\alpha\}^L_\mu=\gamma^L_{l,l'}\cdot\{(\alpha\times\alpha)^{l'},\alpha\}^L_\mu,\ (\gamma^L_{l,l}=1),\qquad(4.33)$$

$$\frac{1}{8}\{\{\alpha,\pi\}^{l'},\alpha\}^L_\mu=\sum_{l=0,2,4}g^L_{l,l'}\cdot\frac{1}{4}\{(\alpha\times\alpha)^l,\pi\}^L_\mu.\qquad(4.34)$$

Values of $\gamma^L_{l,l'}$ and $g^L_{l,l'}$ are given in Appendix A.

As shown in chapter 2, in the GDM method there is one constraint from each even order in the equations of motion. Here in the quartic order the constraint is found as following. Setting $L=2$, keeping only $(D/S)^{(30/21/12/03)}$ and $\Lambda^{(40)}$, $\Lambda^{(22)}_l$, $\Lambda^{(04)}$ terms, $f_{l_L}\times$ Eq.

(4.29) $+\frac{1}{2}\omega^2 \sum_{l=0,2,4} f_l \times$ Eq. (4.31) gives

$$\begin{aligned}
\underline{L=2:} \quad & -i\omega^2 \cdot \Big(\frac{1}{2} \sum_{l=0,2,4} f_l \cdot D^{(21)}_{Ll} + \omega^2 f_{l_L} \cdot D^{(03)}_{L} \Big) \\
&= [\ S^{(00)}\ ,\ \Big(f_{l_L} \cdot D^{(30)}_{L} + \frac{1}{2}\omega^2 \sum_{l=0,2,4} f_l \cdot D^{(12)}_{Ll} \Big)\ ] \\
&\quad + [\ \Big(f_{l_L} \cdot S^{(30)}_{L} + \frac{1}{2}\omega^2 \sum_{l=0,2,4} f_l \cdot S^{(12)}_{Ll} \Big)\ ,\ D^{(00)}\ ] \\
& + 3i\Lambda^{(40)} D^{(01)} \cdot f_0 + \frac{i}{2}\omega^2 \sum_{l=0,2,4} f_l \cdot \Lambda^{(22)}_l D^{(01)} + \ldots
\end{aligned} \tag{4.35}$$

$\frac{1}{2} \sum_{l=0,2,4} f_l \times$ Eq. (4.30) $+\omega^2 f_{l_L} \times$ Eq. (4.32) gives

$$\begin{aligned}
\underline{L=2:} \quad & i \cdot \Big(f_{l_L} \cdot D^{(30)}_{L} + \frac{1}{2}\omega^2 \sum_{l=0,2,4} f_l \cdot D^{(12)}_{Ll} \Big) \\
&= [\ S^{(00)}\ ,\ \Big(\frac{1}{2} \sum_{l=0,2,4} f_l \cdot D^{(21)}_{Ll} + \omega^2 f_{l_L} \cdot D^{(03)}_{L} \Big)\ ] \\
&\quad + [\ \Big(\frac{1}{2} \sum_{l=0,2,4} f_l \cdot S^{(21)}_{Ll} + \omega^2 f_{l_L} \cdot S^{(03)}_{L} \Big)\ ,\ D^{(00)}\ ] \\
& - \frac{i}{2} \sum_{l=0,2,4} f_l \cdot \Lambda^{(22)}_l D^{(10)} - 3i\omega^2 \Lambda^{(04)} D^{(10)} \cdot f_0 + \ldots
\end{aligned} \tag{4.36}$$

where f_l is defined in Eq. (A.7). A solvability condition exists because the variable parts (those including $D^{(30/21/12/03)}$) of Eqs. (4.35) and (4.36) have the same structure as the QRPA equations (4.24) and (4.25).

A computer code is needed for general GDM calculations using realistic forces. This would be a generalization of the existing GDM code for calculations in chapter 3, by including angular-momentum vector coupling. In the next chapter we consider the special case of the quadrupole-plus-pairing Hamiltonian, where approximate *analytical* solutions are possible.

Chapter 5

Quadrupole-plus-Pairing Model

In this chapter the GDM formalism is applied to the specific Hamiltonian of the quadrupole-plus-pairing model. As was understood long ago [20, 21], this model combines the most important nuclear collective phenomena in particle-particle (pairing) and particle-hole (quadrupole mode) channels. Approximate *analytical* solutions exist, if we keep only the coherent part in the interaction, as was usually done for this model. These analytical GDM results are given in Sec. 5.1, and compared with the exact results of the shell model diagonalization in Sec. 5.2. Finally, in Sec. 5.3 we do realistic calculations for tin isotopes.

Let us first introduce the model. The multipole operator is

$$Q^{\dagger}_{\lambda\mu}\{R\} = Tr\{q^{\dagger}_{\lambda\mu}R\} = \sum_{12} q^{\dagger}_{\lambda\mu 12}a^{\dagger}_1 a_2, \tag{5.1}$$

$$q^{\dagger}_{\lambda\mu} = f_\lambda(r)\cdot i^\lambda\, Y_{\lambda\mu}(\theta,\phi), \tag{5.2}$$

where $f_\lambda(r)$ is real. The definition of Eq. (5.2) differs from the "usual" one in two aspects: a factor i^λ is included, and $q^{\dagger}_{\lambda\mu} \sim Y_{\lambda\mu}$ instead of $q_{\lambda\mu}$, thus $q^{\dagger}_{\lambda\mu}$ creates projection μ. The

Hermitian properties are

$$q^\dagger_{\lambda\mu} = (-)^{\lambda-\mu} q_{\lambda\mu}, \quad Q^\dagger_{\lambda\mu} = (-)^{\lambda-\mu} Q_{\lambda\mu}. \tag{5.3}$$

Here we consider only the quadrupole mode, and drop the label $\lambda = 2$. The pairing operators P and $P^\dagger$ are defined by

$$P^\dagger = \frac{1}{2}\sum_1 a^\dagger_1 a^\dagger_{\tilde{1}}, \quad P = \frac{1}{2}\sum_1 a_{\tilde{1}} a_1, \tag{5.4}$$

where $\tilde{1}$ is the time-reversed single-particle level of 1. For fermions, $|\tilde{\tilde{1}}\rangle = -|1\rangle$.

The quadrupole-plus-pairing Hamiltonian is

$$\begin{aligned} H = &\sum_1 (\epsilon_1 - \mu) a^\dagger_1 a_1 - \frac{G}{4}\sum_{12} a^\dagger_1 a^\dagger_{\tilde{1}} a_{\tilde{2}} a_2 \\ &+ \frac{\kappa}{4}\sum_{1234}\sum_\mu (-q^\dagger_{\mu 14} q_{\mu 23} + q^\dagger_{\mu 13} q_{\mu 24}) a^\dagger_1 a^\dagger_2 a_3 a_4. \end{aligned} \tag{5.5}$$

Approximately, this Hamiltonian can be written as $H \approx \sum_1 (\epsilon_1 - \mu) a^\dagger_1 a_1 - G P^\dagger P - \frac{1}{2}\kappa \sum_\mu Q^\dagger_\mu Q_\mu$. The difference is in a one-body term originated from the $Q \cdot Q$ part. H is Hermitian and time-even, which implies real G, κ, and $\epsilon_1 = \epsilon_{\tilde{1}}$. In a realistic nucleus there are protons and neutrons; formally we can still use Eq. (5.5) if the quadrupole force strengths are the same for proton-proton, neutron-neutron, and proton-neutron interactions ($\kappa_p = \kappa_n = \kappa_{pn} = \kappa$), while remembering the pairing is treated for protons and neutrons separately ($G_p \neq G_n$). We will assume this is the case.

5.1 The GDM Method

In this section the GDM equations of motion of chapter 4 are solved in the quadrupole-plus-pairing model. As was usually done, only the "coherent" part of the interaction is kept: we neglect in the $W\{R\}$ field (4.3) the Fock/exchange terms and the contribution from the pairing force, and in the $\Delta\{K\}$ field (4.4) the contribution from the quadrupole-quadrupole force. Then the results are analytical:

$$W\{R\}_{12} \approx -\kappa \sum_{\mu} q^{\dagger}_{\mu 12} Q_{\mu}, \tag{5.6}$$

$$\Delta\{K\}_{12} \approx \delta_{1\tilde{2}} GP. \tag{5.7}$$

5.1.1 BCS Theory

In the quadrupole-plus-pairing model the HFB equation becomes the BCS equation. The canonical transformation (4.21) mixes only time-reversal pair of orbitals,

$$u_{12} = \delta_{12} u_1, \quad v_{12} = -\delta_{1\tilde{2}} v_1, \quad (u_1)^2 + (v_1)^2 = 1, \tag{5.8}$$

where $u_1 = u_{\tilde{1}}$, $v_1 = v_{\tilde{1}}$ are real numbers. The density matrices (4.22) become

$$\rho_{12} = \delta_{12} (v_1)^2, \quad \kappa_{12} = \delta_{1\tilde{2}} u_1 v_1. \tag{5.9}$$

The constant terms of Eq. (5.6) give

$$f\{\rho\}_{12} = \delta_{12}[\epsilon_1 - \mu] + w^{(00)}_{12} \approx \delta_{12}[\epsilon_1 - \mu - G(v_1)^2] \equiv \delta_{12} e_1, \tag{5.10}$$

where $e_1 \equiv \epsilon_1 - \mu - G(v_1)^2$. And the constant terms of Eq. (5.7) give

$$\Delta\{\kappa\}_{12} \approx \delta_{1\tilde{2}}\, GP^{(00)} \equiv -\delta_{1\tilde{2}}\, \Delta, \tag{5.11}$$

where the pairing energy $\Delta \equiv -GP^{(00)} = \frac{G}{2}\sum_3 u_3 v_3$. Then the HFB equation (4.19) leads to the BCS set of equations:

$$\Delta \cdot \Big(1 - \frac{G}{4} \sum_1 \frac{1}{E_1} \Big) = 0, \tag{5.12}$$

$$e_1 = \epsilon_1 - \mu - G(v_1)^2, \tag{5.13}$$

$$E_1 = \sqrt{(e_1)^2 + (\Delta)^2}, \tag{5.14}$$

$$(u_1)^2 = \frac{1}{2}\left(1 + \frac{e_1}{E_1}\right), \quad (v_1)^2 = \frac{1}{2}\left(1 - \frac{e_1}{E_1}\right), \tag{5.15}$$

$$N = \sum_1 (v_1)^2. \tag{5.16}$$

E_1 is the quasiparticle energy. The chemical potential μ is fixed by Eq. (5.16). The gap equation (5.12) has a non-trivial solution $\Delta > 0$ only if G is greater than its critical value G_c [21]. For later convenience we introduce:

$$\xi^{(2)}_{\mu 12} \equiv \frac{(u_1 v_2 + u_2 v_1)}{(E_1 + E_2)^2} q_{\mu 12},\ \eta_{\mu 12} \equiv (u_1 u_2 - v_1 v_2) q_{\mu 12}. \tag{5.17}$$

The superscript "(2)" in $\xi^{(2)}_{\mu 12}$ stands for the denominator $1/(E_1 + E_2)^2$, other "powers" are defined similarly.

5.1.2 Quasi-Particle Random Phase Approximation

Here we give only the final results. Detailed derivations can be found in Ref. [12]. The QRPA secular equation determining frequency ω^2 is

$$1 = \kappa \sum_{\tau_1 j_1 \tau_2 j_2} (-)^{j_2 - j_1} \frac{\sqrt{(2j_1+1)(2j_2+1)}}{5} \frac{E_1 + E_2}{(E_1+E_2)^2 - \omega^2} \, \xi^\dagger_{\|12} \xi^\dagger_{\|21}. \tag{5.18}$$

$\xi^\dagger_{\|12} \equiv \langle \tau_1 j_1 \| \xi^\dagger \| \tau_2 j_2 \rangle$ is the reduced matrix element, the convention for which is given in Appendix B. τ_1 combines all other quantum numbers specifying a single-particle level, except j_1. The normalization $Q^{(10)}$ is given by

$$1 = (\kappa Q^{(10)})^2 \sum_{\tau_1 j_1 \tau_2 j_2} (-)^{j_2 - j_1} \frac{\sqrt{(2j_1+1)(2j_2+1)}}{5} \frac{(E_1 + E_2)}{[(E_1+E_2)^2 - \omega^2]^2} \, \xi^\dagger_{\|12} \xi^\dagger_{\|21}. \tag{5.19}$$

Starting from the next (cubic) order, we restrict ourselves to regions near the critical point of QRPA ($\omega^2 \approx 0$). Following the procedure in Appendix C, we give results of $\Lambda^{(30)}$ and $\Lambda^{(40)}$ in their leading order of ω^2 (constant terms independent of ω^2). As in the Landau phase transition theory, the critical point is such a position that the leading potential term $\omega^2 \alpha^2/2$ happens to vanish. The next non-vanishing term, usually $\Lambda^{(40)} \alpha^4/4$, is thus dominant restoring the stability of the system (see Refs. [15] and [12]).

5.1.3 Cubic Anharmonicity

In this model the cubic anharmonicity (C.7) becomes

$$\Lambda^{(30)} \doteq 3(\kappa Q^{(10)})^3 \sum_{\tau_1 j_1 \tau_2 j_2 \tau_3 j_3} \sqrt{\frac{(2j_1+1)(2j_2+1)(2j_3+1)}{5}} \cdot \begin{Bmatrix} 2 & 2 & 2 \\ j_1 & j_2 & j_3 \end{Bmatrix} \cdot \xi^{(1)\dagger}_{\|12}\ \xi^{(1)\dagger}_{\|23}\ \eta^{\dagger}_{\|31}, \tag{5.20}$$

where $\doteq$ means the equation is correct in constant terms but not in ω^2 terms or higher.

We give the expression of $P^{(20)}$ which will appear in $\Lambda_c^{(40)}$ of next section:

$$P^{(20)} \cdot [\ 1 - G \sum_{\tau_1 j_1} (2j_1+1) \frac{[(u_1)^2 - (v_1)^2]^2}{4E_1}\ ] \doteq$$
$$-(\kappa Q^{(10)})^2 \sum_{\tau_1 j_1 \tau_2 j_2} (-)^{j_1+j_2} \sqrt{\frac{(2j_1+1)(2j_2+1)}{5}}$$
$$\cdot \Big[\ 2u_1 v_1 \cdot \xi^{(1)\dagger}_{\|12} \xi^{(1)\dagger}_{\|21} - \frac{(u_1)^2 - (v_1)^2}{E_1} \cdot \eta^{\dagger}_{\|12} \xi^{(1)\dagger}_{\|21}\ \Big]. \tag{5.21}$$

$P^{(20)}$ is divergent when G is greater than but close to G_c. In this region of the pairing phase transition, Δ is small, and $P^{(20)} \sim 1/\Delta$. The GDM + BCS method is not valid in this region: in the mean-field order the BCS solution already fails, as is well known.

5.1.4 Quartic Anharmonicity

The quartic anharmonicity Eq. (C.8) becomes

$$
\begin{aligned}
f_0 \cdot \Lambda^{(40)} \doteq -2\ f_2 \cdot (\kappa Q^{(10)})^2 (\Lambda^{(30)})^2\ \mathrm{Tr}\Big[\xi_\mu \xi_\mu^{(5)\dagger}\Big] - f_2 \cdot \Lambda^{(30)} \Lambda^{(12)} \\
-f_2 \cdot \Lambda^{(30)} (\kappa Q^{(10)})^3 \Big(\ \mathrm{Tr}\Big[\{\xi^{(1)}, \xi^{(3)}\}_\mu^{L=2} \eta_\mu^\dagger\Big] + \mathrm{Tr}\Big[\{\eta, \xi^{(3)}\}_\mu^{L=2} \xi_\mu^{(1)\dagger}\Big] \\
+2\ \mathrm{Tr}\Big[\{\eta, \xi^{(1)}\}_\mu^{L=2} \xi_\mu^{(3)\dagger}\Big] + \mathrm{Tr}\Big[\{\eta, \xi^{(2)}\}_\mu^{L=2} \xi_\mu^{(2)\dagger}\Big]\ \Big) \\
-f_0 \cdot G\ P^{(20)} (\kappa Q^{(10)})^2 \sum_{12} (u_1 v_1 + u_2 v_2)\ \xi_{\mu 12} \xi_{\mu 21}^{(2)\dagger} \\
+f_0 \cdot G\ P^{(20)} (\kappa Q^{(10)})^2 \cdot \sum_{12} \{ \frac{(u_1)^2 - (v_1)^2}{2E_1} + \frac{(u_2)^2 - (v_2)^2}{2E_2} \} \xi_{\mu 12}^{(1)} \eta_{\mu 21}^\dagger \\
+(\kappa Q^{(10)})^4 \sum_{l=0,2,4} f_l \cdot \Big(\mathrm{Tr}\Big[\{\xi, (\xi^{(1)} \times \xi^{(1)})^l\}_\mu^{L=2} \xi_\mu^{(1)\dagger}\Big] \\
-\mathrm{Tr}\Big[\{\eta, \{\eta, \xi^{(1)}\}^{l,(1)}\}_\mu^{L=2} \xi_\mu^{(1)\dagger}\Big] - \mathrm{Tr}\Big[\{\xi^{(1)}, \{\eta, \xi^{(1)}\}^{l,(1)}\}_\mu^{L=2} \eta_\mu^\dagger\Big]\ \Big), \qquad (5.22)
\end{aligned}
$$

where $\{\eta, \xi^{(1)}\}_{12}^{l,(1)} = \{\eta, \xi^{(1)}\}_{12}^{l} / (E_1 + E_2)$. There is an undetermined parameter $\Lambda^{(12)}$ in Eq. (5.22). Values of numerical factors f_l are given in Appendix A. Equation (5.22) in terms of reduced matrix elements can be found in Ref. [12].

5.2 Comparison with Exact Results

We compare the GDM results of Sec. 5.1 in the following model with the exact one of NuShellX [22]. There are 10 fermions of one kind and four single-particle levels with energies:

single − particle levels	$1p\frac{1}{2}$	$0f\frac{7}{2}$	$1p\frac{3}{2}$	$0f\frac{5}{2}$
ϵ (MeV)	−0.1	0.0	1.0	1.1

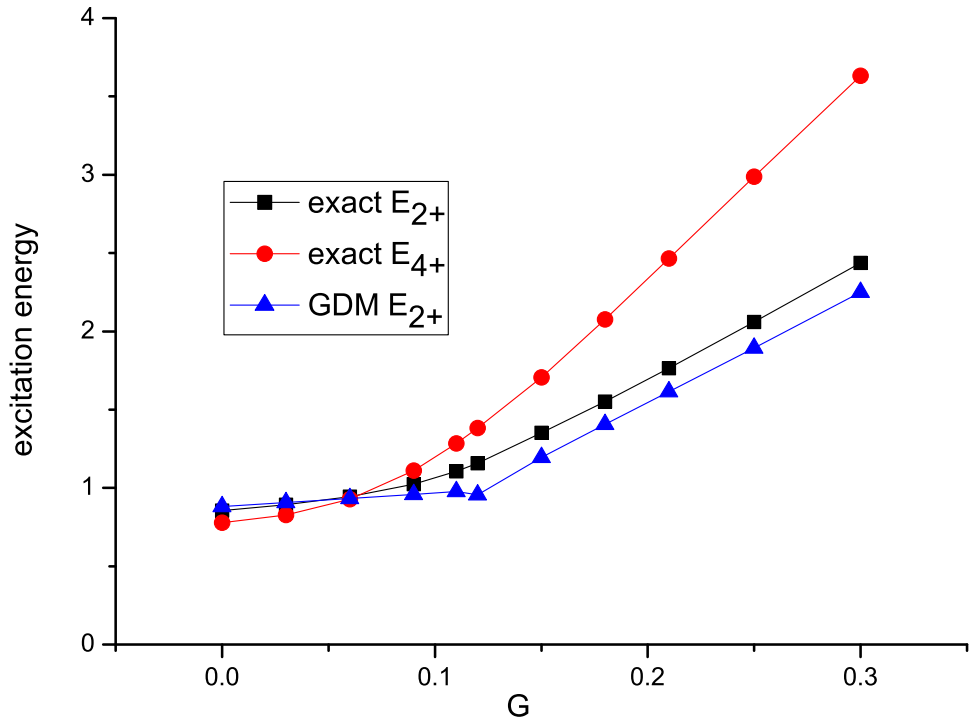

Figure 5.1: Excitation energies (from Table 5.1) in the quadrupole plus pairing model as a function of the pairing strength G, at the critical point $\omega = 0$ ($\kappa = \kappa_c$). The black squares and red circles show the exact excitation energy of the first 2^+ and 4^+ state, respectively, "NuShellX E_{2+}" and "NuShellX E_{4+}" in Table 5.1. The blue triangles give "GDM E_{2+}" from Table 5.1.

We take the radial wavefunctions to be harmonic oscillator ones. In Eq. (5.2) we take $f(r)$ to be r^2 so $q^\dagger_\mu = -\hat{r}^2 Y_{2\mu}(\hat{\theta}, \hat{\phi})$. For convenience we make $q^\dagger_\mu$ dimensionless by combining its original dimension with κ (see the end of Appendix B). The model space is similar to the realistic pf-shell, but the $1p\frac{1}{2}$ and $1p\frac{3}{2}$ levels are inverted to increase collectivity: in the current case the q matrix elements ($q_{1p\frac{1}{2},0f\frac{5}{2}}$ and $q_{1p\frac{3}{2},0f\frac{7}{2}}$) are large between the single-particle levels above and below the Fermi surface.

We restrict ourselves to the critical region (QRPA $\omega^2 \approx 0$). As said in Sec. 5.1.2, here the stability of the system is restored by the quartic potential term $\Lambda^{(40)}\alpha^4/4$. We did a set

Table 5.1: Results of the quadrupole plus pairing model for different values of the pairing strength G. All quantities are in units of MeV. Δ is the solution of Eq. (5.12). The chemical potential μ is the solution of Eq. (5.16). κ_c is the critical κ such that ω^2 in Eq. (5.18) becomes zero. $\Lambda^{(30)}$ is given by Eq. (5.20). $\Lambda^{(40)}$ is given by Eq. (5.22) setting $\Lambda^{(12)} = 0$. "GDM E_{2+}" is the excitation energy of the first 2^+ state from diagonalizing Eq. (4.18) for $\omega^2 = \Lambda^{(12)} = \Lambda^{(04)} = \Lambda_L^{(22)} = 0$. "NuShellX E_{2+}" is the exact excitation energy of the first 2^+ state from diagonalizing Eq. (5.5), in which G and κ are given by G and κ_c in the table. Similarly, "NuShellX E_{4+}" is the exact excitation energy of the first 4^+ state.

G	0	0.03	0.06	0.09	0.11	0.12
Δ	0.0	0.0	0.0	0.0	0.0	0.066
μ	0.5	0.5	0.5	0.5	0.5	0.454
κ_c	0.102	0.105	0.107	0.110	0.112	0.113
$\Lambda^{(30)}$	-0.160	-0.173	-0.188	-0.203	-0.213	-0.219
$\Lambda^{(40)}$	0.483	0.526	0.572	0.621	0.655	0.616
GDM E_{2+}	0.882	0.908	0.933	0.959	0.976	0.955
NuShellX E_{2+}	0.855	0.892	0.944	1.023	1.106	1.158
NuShellX E_{4+}	0.778	0.827	0.927	1.110	1.284	1.383

G	0.15	0.18	0.21	0.25	0.30
Δ	0.453	0.672	0.862	1.096	1.374
μ	0.444	0.429	0.415	0.395	0.370
κ_c	0.113	0.122	0.135	0.154	0.179
$\Lambda^{(30)}$	-0.234	-0.270	-0.310	-0.378	-0.474
$\Lambda^{(40)}$	1.185	1.918	2.901	4.683	7.830
GDM E_{2+}	1.194	1.405	1.614	1.894	2.249
NuShellX E_{2+}	1.353	1.552	1.764	2.059	2.438
NuShellX E_{4+}	1.705	2.076	2.465	2.987	3.631

of calculations with increasing pairing strength G. At each value of G, the strength κ of the $Q \cdot Q$ force is taken to be at the critical value κ_c such that the QRPA frequency $\omega^2 = 0$. The results are summarized in Table 5.1. For clarity, we draw the last three lines of Table 5.1 as Fig. 5.1. The coefficient $\Lambda^{(40)}$ in Table 5.1 is calculated by Eq. (5.22) setting $\Lambda^{(12)} = 0$ (dropping the $-f_2 \cdot \Lambda^{(30)}\Lambda^{(12)}$ term). A non-zero term $\Lambda^{(12)}$ in its reasonable range does not influence $\Lambda^{(40)}$ much, since in the current model $\Lambda^{(30)}$ is small due to the approximate symmetry with respect to the Fermi surface (see Table 5.1). Then "GDM E_{2^+}" is calculated by diagonalizing Eq. (4.18), setting $\Lambda^{(12)} = \Lambda^{(04)} = \Lambda_L^{(22)} = 0$ ($\omega^2 = 0$ since κ takes its critical value).

The critical value of the pairing strength G_c is around $0.11 \sim 0.12$ MeV. When $G < G_c$, the BCS solution $\Delta = 0$, and μ can be anywhere between $\epsilon_{0f\frac{7}{2}} = 0$ and $\epsilon_{1p\frac{3}{2}} = 1.0$ MeV. We checked that in this case our results (5.18-5.22) do not depend on the choice of μ. In Table 5.1 we fix μ at 0.5 MeV. In the region where G is greater than but close to G_c, our method is invalid as discussed under Eq. (5.21). This is illustrated in Fig. 5.1 by the 'kink' on the "GDM E_{2^+}" curve near $G \sim 0.12$.

In Fig. 5.1 "exact E_{2^+}" and "exact E_{4^+}" are the exact results by NuShellX. At $G = 0$ the first excited state is 4^+ instead of 2^+. In this case the 4^+ state is a single-particle excitation from $0f\frac{7}{2}$ to $0f\frac{5}{2}$; the 2^+ state is a collective state with approximately half holes in $1p\frac{1}{2}$ and $0f\frac{7}{2}$ levels, half particles in $1p\frac{3}{2}$ and $0f\frac{5}{2}$. As G increases, the collective 2^+ state becomes the first excited state. When G is large enough, Δ dominates over the original single-particle spacing ϵ, and the results become stable. As an example, at $G = 0.30$ MeV, the quasiparticle continuum starts at ~ 3.5 MeV; from the second excited state 0^+ at 3.506 MeV to 4.153 MeV there are 15 states with $J^P = 0^+, 2^+, 4^+, 6^+$. The first excited state 2^+

at 2.438 MeV should be identified as a collective state, stabilized at around sixty percents within the gap.

It is seen in Fig. 5.1 that "GDM E_{2^+}" agrees well with the exact result "exact E_{2^+}" in general. On the $G < G_c$ side, our E_{2^+} does increase with G although not rapidly enough. On the $G > G_c$ side, when Δ is not too small, the agreement is very good.

Table 5.2: Neutron single-particle energies for ^{100}Sn and ^{132}Sn in units of MeV.

s.p. level	$0g\frac{9}{2}$	$0g\frac{7}{2}$	$1d\frac{5}{2}$	$1d\frac{3}{2}$	$2s\frac{1}{2}$	$0h\frac{11}{2}$	$0h\frac{9}{2}$
^{100}Sn	-16.7893	-10.2893	-10.6089	-8.6944	-8.7167	-8.8152	-0.8152
^{132}Sn	-14.74	-9.74	-8.97	-7.31	-7.62	-7.38	-0.38

5.3 Tin isotopes

As a realistic application of the GDM formalism, we consider tin isotopes. They are semi-magic nuclei; the proton number 50 is a magic number. In our calculations the protons are kept inactive. For the neutrons, we keep 7 active single-particle levels: $0g\frac{9}{2}$, $0g\frac{7}{2}$, $1d\frac{5}{2}$, $1d\frac{3}{2}$, $2s\frac{1}{2}$, $0h\frac{11}{2}$, and $0h\frac{9}{2}$. Their energies for ^{100}Sn and ^{132}Sn are listed in Table 5.2. These energies are taken from two shell-model calculations in Refs. [23] and [24]. For tin isotopes with mass number from 102 to 130, the single-particle energies are given by linear extrapolation between the above two ends ^{100}Sn and ^{132}Sn. We assume that their wavefunctions are of the harmonic oscillator type, and the matrix elements of the quadrupole operator $q^\dagger_\mu = -r^2 Y_{2\mu}$ are given in appendix B. The results have the factor b^2, where the length parameter $b = \sqrt{\hbar/(m\Omega_0)}$ characterize the size of the harmonic oscillator wavefunction, Ω_0 is the frequency of the harmonic mean field. In our calculation we take $\hbar\Omega_0 = 45A^{-1/3} - 25A^{-2/3}$ MeV, suggested in Ref. [25], fitting globally the radii of the nuclei. The variations of $\hbar\Omega_0$ are small along the tin isotope chain, from 8.53 MeV for ^{100}Sn to 7.87 MeV for ^{132}Sn.

The strength G of the pairing interaction in the Hamiltonian (5.5) is fixed to be 0.175 MeV, reproducing the even-odd mass staggering. In Fig. 5.2 we plot the experimental even-odd mass staggering and the BCS pairing gap Δ. Near the neutron magic numbers (^{102}Sn, ^{130}Sn), the BCS theory incorrectly gives a too small solution, as is well known. Thus in the following we only consider isotopes from ^{104}Sn to ^{128}Sn.

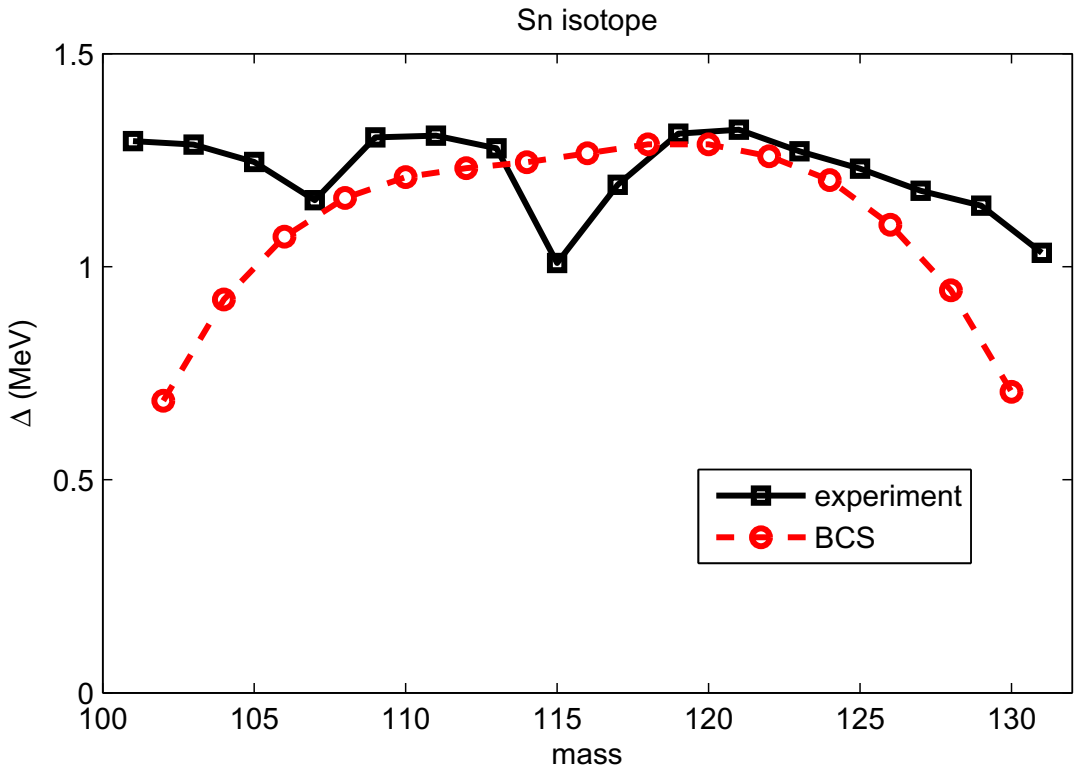

Figure 5.2: Even-odd mass staggering in the tin isotopes. The black squares show the experimental data $M_A - (M_{A-1} + M_{A+1})/2$. The red circles show the BCS pairing gap Δ as the solution of Eq. (5.12).

The strength κ of the quadrupole interaction in the Hamiltonian (5.5) is fixed to be $\kappa b^4 = 0.13$ MeV, where b is the above mentioned harmonic-oscillator length parameter. The above value of κ reproduces in the QRPA calculation the experimental $E(2^+)$ at the two ends (^{104}Sn and ^{128}Sn) of the tin isotope chain (see Fig. 5.3). In the middle, as the number of valence particle increases, the QRPA frequency ω^2 becomes small and finally negative, with increasing collectivity.

In the GDM calculation, we calculate $\Lambda^{(30)}$ and $\Lambda^{(40)}$ in their leading constant term in the expansion over ω^2, through Eqs. (5.20) and (5.22). The resulting Hamiltonian,

$$H = \frac{\omega^2}{2}\sqrt{5}(\alpha\times\alpha)^0_0 + \frac{1}{2}\sqrt{5}(\pi\times\pi)^0_0 + \frac{\Lambda^{(30)}_c}{6}\sqrt{5}\{(\alpha\times\alpha)^2,\alpha\}^0_0 + \frac{\Lambda^{(40)}_c}{4}\sqrt{5}((\alpha\times\alpha)^0\times(\alpha\times\alpha)^0)^0_0, \tag{5.23}$$

is diagonalized in the "physical bosonic space" $\{|0 \le n \le n_{\max}\rangle\}$, defined in the same way as that in chapter 3. Specifically, $|n\rangle$ is the state with n phonons, $\sum_\mu A^\dagger_\mu A_\mu |n\rangle = n|n\rangle$, where $A^\dagger_\mu$ is defined by generalizations of Eqs. (3.5) and (3.11). The maximal number of phonons, $n_{\max}$, is given by the smaller of the number of pairs of valence particles or holes in the $50-82$ shell. For example, $n_{\max} = 5$ for ^{110}Sn and $n_{\max} = 6$ for ^{120}Sn.

In the Hamiltonian (5.23), $\Lambda^{(30)}$ and $\Lambda^{(40)}$ are calculated only in their leading order of ω^2. However, it should be a good approximation because here the small parameter $\omega^2/(2\Delta)^2$ is around 0.3. As explained in appendix C, anharmonicities $\Lambda^{(mn)}$ should be smooth functions of ω^2, in such a small range ~ 0.3 their variations are usually small. This is the case for the models in chapter 3. The Hamiltonian (5.23) is expected to work better with increasing collectivity. Here in Fig. 5.3 we show the GDM results from ^{108}Sn to ^{124}Sn, where $n_{\max} \ge 4$. Near magic numbers where $n_{\max} \le 3$, it may be not meaningful to speak about quartic

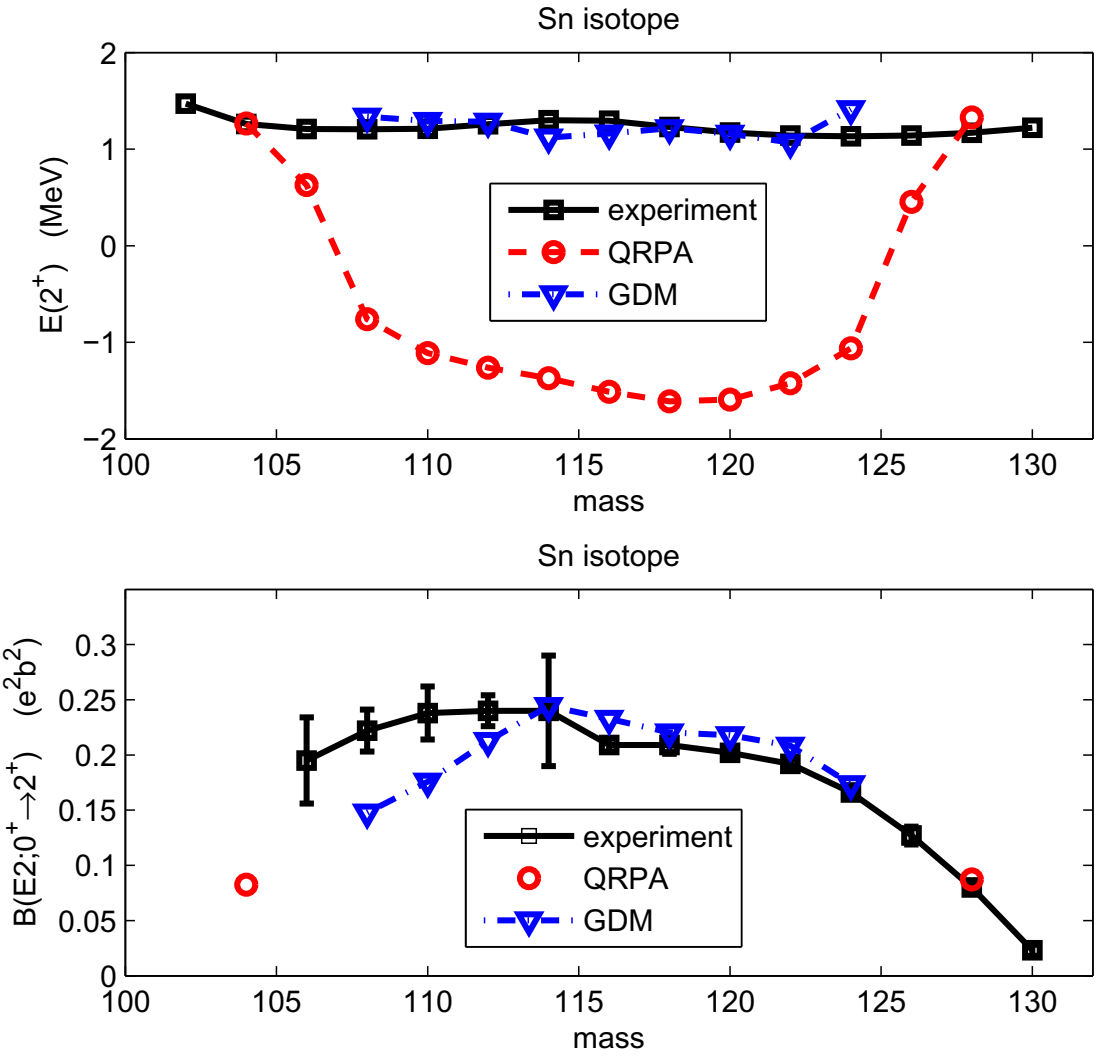

Figure 5.3: Excitation energy $E(2^+)$ and transition rates $B(E2; 0^+ \rightarrow 2^+)$ for the first excited state 2^+ in the tin isotopes. The black squares show the experimental data taken from Ref. [26]. The blue triangles are the GDM results. The red circles show the QRPA results. On the upper panel, negative values for the QRPA $E(2^+)$ actually mean imaginary frequency.

anharmonicity in the Hamiltonian (5.23).

In Fig. 5.3 we see that the GDM calculation with the Hamiltonian (5.23) reproduces the experimental data quite well in the region ^{108}Sn $\sim$ ^{124}Sn, where the QRPA solution collapses (negative ω^2). The quartic potential term $\Lambda^{(40)}\alpha^4$ restores the stability of the system. In the lower panel we calculate the transition rates (defined in appendix B) of the quadrupole operator $Q_\mu \approx Q^{(10)}\alpha_\mu$, with $Q^{(10)}$ given by Eq. (5.19). An effective charge $e_{\text{eff}} = 0.7$ is used in both the QRPA and the GDM calculations.

The key point here is that the residual interaction, $\kappa Q^\dagger Q$ and $GP^\dagger P$, should be smooth. Consequently in the middle of the shell the QRPA solution collapses as a result of increasing collectivity. A recent QRPA calculation with Skyrme interactions shows quite a similar pattern [27]. In this region higher order anharmonicities, here mainly $\Lambda^{(40)}$, restore the stability of the system.

Chapter 6

Conclusion

This work develops the generalized density matrix (GDM) formalism for microscopic calculation of the collective/bosonic Hamiltonian. The standard method in nuclear structure, shell model, requires impractical computation time for majority of medium and heavy nuclei. Thus, we have to look for physically justified approximations by identifying the most important degrees of freedom out of the huge shell-model space. The collective modes, like vibration or rotation of the nucleus as a whole, are definitely the correct choice for describing the low-lying spectrum. These collective modes have the nature of bosons; phenomenological models using an effective bosonic Hamiltonian are often quite successful in explaining the experimental data. However, the complete microscopic theory of deriving the collective/bosonic Hamiltonian from the underlying shell-model Hamiltonian is still missing after several decades.

In this work we propose a procedure based on the generalized density matrix. The procedure is rather simple, clean, and consistent. In compact form, there are only two equations, (2.14) and (2.33). They fix the bosonic Hamiltonian completely, which greatly

generalizes the well-known random phase approximation that calculates only the harmonic terms. Many nuclei, including those at the γ-unstable and rotational limit, have a small or negative harmonic potential, thus the anharmonic terms are indispensable restoring the stability of the system. Specifically, we show that deformation can be described without breaking the rotational symmetry in the mean field (cranking); relevant correlations are put in "dynamically" at higher orders. Thus the GDM approach is suitable to describe such phenomena as shape fluctuations and coexistence, also in the transitional region the coupling between rotational and vibrational motions.

In this thesis, the test of the proposed GDM method in its most general form has been limited to systems without rotational symmetry (chapter 3). The agreement with the exact results, both for energies and transition rates, is very good. The application to realistic nuclei has only been done for the "analytical" quadrupole-plus-pairing model near the critical region of the quasi-particle random phase approximation (chapter 5). The next step would be generalizing the existing GDM code by including angular-momentum vector coupling that are necessary for general realistic calculations.

As a systematic way to construct the effective Hamiltonian, the applicability of the GDM formalism should be more broad. We list here some future directions. Firstly, it may be possible to develop a theory for pairing without introducing Bogoliubov quasi-particles, which improves the BCS or Hartree-Fock-Bogoliubov treatment in the sense that the exact particle number is always conserved. The current available results seem promising. Secondly, the GDM formalism could be used to construct the effective Hamiltonian for odd-mass nuclei, where the coupling between the collective modes and the unpaired nucleon is very important (see appendix E). Thirdly, a more ambitious project would be doing better GDM calculations

for the even-even nuclei by decoupling two or more nucleons from the collective modes. In this way the "single-particle" states could be studied and collective states should be more accurate. From the computational/mathematical point of view, the GDM formalism should be identical to the shell model if all the nucleons are decoupled from the collective modes. Practically, we could seek to do the best calculation allowed by computer time. The odd-mass and odd-odd nuclei could be treated along the same line.

Of course, the vitality of the GDM method depends on the results. But we hope that the current work could serve as a beginning of its promising future.

APPENDICES

Appendix A

Values of $g^L_{l,l'}$ and $\gamma^L_{l,l'}$

The definition of $g^L_{l,l'}$ is given by Eq. (4.34),

$$\frac{1}{8}\{\{\alpha,\pi\}^{l'},\alpha\}^L_\mu = \sum_{l=0,2,4} g^L_{l,l'}\cdot\frac{1}{4}\{(\alpha\times\alpha)^l,\pi\}^L_\mu,$$

which implies

$$g^L_{l,l'} = (-)^{l-l'}\sqrt{(2l+1)(2l'+1)}\begin{Bmatrix} 2 & 2 & l \\ 2 & L & l' \end{Bmatrix} = g^L_{l',l}. \tag{A.1}$$

The definition of $\gamma^L_{l,l'}$ is given by Eq. (4.33),

$$\{(\alpha\times\alpha)^l,\alpha\}^L_\mu = \gamma^L_{l,l'}\cdot\{(\alpha\times\alpha)^{l'},\alpha\}^L_\mu.$$

Analytical expressions of $\gamma^L_{l,l'}$ can be obtained in the following way. Assume l and l' are *even*. We have the identity

$$\begin{aligned}
&[\ \{(\alpha^\dagger \times \alpha^\dagger)^{l'}, \alpha^\dagger\}^L_\mu\ ,\ (\pi \times \pi)^0_0\ ]\ |^{L=0,2,3,4,6}_{l'=0,2,4} \\
&= i\frac{2}{\sqrt{5}} \sum_{l=0,2,4} (\ \delta_{l,l'} + 2 \cdot g^L_{l,l'}\ ) \cdot \{(\alpha^\dagger \times \alpha^\dagger)^l, \pi^\dagger\}^L_\mu. \qquad \text{(A.2)}
\end{aligned}$$

Replacing l' in Eq. (A.2) by l'' we obtain

$$\begin{aligned}
&[\ \{(\alpha^\dagger \times \alpha^\dagger)^{l''}, \alpha^\dagger\}^L_\mu\ ,\ (\pi \times \pi)^0_0\ ]\ |^{L=0,2,3,4,6}_{l''=0,2,4} \\
&= i\frac{2}{\sqrt{5}} \sum_{l=0,2,4} (\ \delta_{l,l''} + 2 \cdot g^L_{l,l''}\ ) \cdot \{(\alpha^\dagger \times \alpha^\dagger)^l, \pi^\dagger\}^L_\mu. \qquad \text{(A.3)}
\end{aligned}$$

Let us take the ratio of Eq. (A.2)/Eq. (A.3). The left-hand side is $\gamma^L_{l',l''}$ by Eq. (4.33). Since in the right-hand side of Eq. (A.2) and Eq. (A.3), $\{(\alpha^\dagger \times \alpha^\dagger)^l, \pi^\dagger\}^L_\mu$ with different l are linearly independent, we have

$$\gamma^L_{l',l''} = \frac{\delta_{l,l'} + 2 \cdot g^L_{l,l'}}{\delta_{l,l''} + 2 \cdot g^L_{l,l''}}, \quad (l = 0, 2, 4). \qquad \text{(A.4)}$$

The ratio on the right-hand side is independent of l. Since the matrix $\delta_{l,l'} + 2 \cdot g^L_{l,l'}$ is symmetric (with respect to l, l'), Eq. (A.4) implies

$$\delta_{l,l'} + 2 \cdot g^L_{l,l'} = f^L_l \cdot f^L_{l'}, \qquad \text{(A.5)}$$

where $f_l^L = \sqrt{1 + 2 \cdot g_{l,l}^L}$. Then from Eq. (A.4) we obtain

$$\gamma_{l',l''}^L = \frac{f_{l'}^L}{f_{l''}^L}. \tag{A.6}$$

We will use only $L = 2$:

$$f_{l=0}^{L=2} = \sqrt{\frac{7}{5}}, \quad f_{l=2}^{L=2} = \frac{2}{\sqrt{7}}, \quad f_{l=4}^{L=2} = \frac{6}{\sqrt{35}}. \tag{A.7}$$

In the main text the superscript $^{L=2}$ on $f_l^{L=2}$ is dropped for simplicity.

Appendix B

Conventions

Our convention for the Wigner-Eckart theorem is:

$$\langle n_1 j_1 m_1 | T^\lambda_\mu | n_2 j_2 m_2 \rangle = C^{j_1 m_1}_{j_2 m_2, \lambda\mu} \cdot \langle n_1 j_1 \| T^\lambda \| n_2 j_2 \rangle, \tag{B.1}$$

where $C^{j_1 m_1}_{j_2 m_2, \lambda\mu}$ is the Clebsch-Gordan coefficients.

The reduced matrix element of $q^\dagger_{\lambda\mu}$ (5.2) is

$$\langle nlj \| q^\dagger_\lambda \| n'l'j' \rangle =$$
$$\begin{cases} i^{l'+\lambda-l}(-)^{j'+\lambda-j}\sqrt{\frac{(2\lambda+1)(2j'+1)}{4\pi(2j+1)}} \cdot C^{j\frac{1}{2}}_{j'\frac{1}{2},\lambda 0} \int dr\ r^2 f_\lambda(r) R_{nlj}(r) R_{n'l'j'}(r), & l'+\lambda-l \text{ is even}, \\ 0, & l'+\lambda-l \text{ is odd}, \end{cases}$$

where the single-particle wave functions $|nljm\rangle$ are defined as

$$\psi_{nljm} = R_{nlj}(r) \cdot \sum_{m_l m_s} C^{jm}_{lm_l, sm_s}\ i^l Y_{lm_l}(\theta, \phi)\ \chi_{m_s},$$

in which spin $s = \frac{1}{2}$, $R_{nlj}(r)$ is a real function, and a factor i^l is included.

In this work we have used the matrix elements of the realistic quadrupole operator in the harmonic oscillator single-particle basis. In this case $\lambda = 2$, $f_\lambda(r) = r^2$, $R_{nlj}(r)$ is independent of j, and $n = 2n_r + l$ is the major-shell quantum number. The non-vanishing matrix elements of $\langle nlj\|q^\dagger\|n'l'j'\rangle$ have $n - n' = -2, 0, 2$, and $l - l' = -2, 0, 2$. For these combinations the symmetric radial integral becomes

$$\int dr\ r^4 R_{nl}(r) R_{n'l'}(r) = b^2 \cdot \begin{cases} n + \frac{3}{2}, & n' = n,\ l' = l, \\ -\sqrt{(n+l+3)(n-l)}, & n' = n,\ l' = l+2, \\ -\frac{1}{2}\sqrt{(n+l+3)(n-l+2)}, & n' = n+2,\ l' = l, \\ \frac{1}{2}\sqrt{(n+l+3)(n+l+5)}, & n' = n+2,\ l' = l+2, \\ \frac{1}{2}\sqrt{(n-l+2)(n-l+4)}, & n' = n+2,\ l' = l-2, \end{cases}$$

where $b = \sqrt{\frac{\hbar}{m\Omega_0}}$ is the length parameter, Ω_0 is the harmonic oscillator frequency. As mentioned at the beginning of Sec. 5.2, the factor b^2 will be combined with κ to make $q^\dagger_\mu$ dimensionless.

The transition rates B(E2) is defined as

$$B(E2, J_i \to J_f) = \frac{2J_f + 1}{2J_i + 1} |\langle f\|Q\|i\rangle|^2 \tag{B.2}$$

In Fig. 5.3 the unit of $B(E2, 0^+ \to 2^+)$ is given in e^2b^2, where $1b = 1\text{barn} = 100\text{fm}^2$.

Appendix C

Systems Near Critical Point

Anharmonicities become important when the harmonic potential $\omega^2\alpha^2/2$ becomes small or negative. This is the case in realistic medium and heavy nuclei away from magic numbers [28]. In the critical region $\omega^2 \approx 0$, we are able to determine the cubic potential term $\Lambda^{(30)}$ and the quartic potential term $\Lambda^{(40)}$ as shown below.

We make an assumption in the spirit of Landau phase transition theory: in Eq. (2.4), the leading potential term $\omega^2\alpha^2/2$ vanishes at the critical point, while other higher order terms $\Lambda^{(mn)}$ remain *finite*. Taylor expanding $\Lambda^{(mn)}$ over ω^2,

$$\Lambda^{(mn)} = \Lambda_c^{(mn)} + \Lambda_1^{(mn)}\omega^2 + \Lambda_2^{(mn)}\omega^4 + \ldots, \tag{C.1}$$

the leading constant term $\Lambda_c^{(mn)}$ is finite. The stability of the system is restored by higher order anharmonicities, e.g. $\Lambda^{(40)}\alpha^4/4$; thus the generalized density matrices $r_{12}^{(mn)}$ are also finite. Again we call the finite leading constant term in a Taylor expansion $r_{c12}^{(mn)}$. For convenience, we use $\doteq$ instead of $=$ if an equation is correct in constant terms but not in ω^2 terms or higher.

C.1 Harmonic Order

Keeping only the constant terms of Eq. (2.23) we have

$$w_{34}^{(10)} \doteq \sum_{12} V_{3214} \frac{n_{12}}{e_{12}} \; w_{12}^{(10)}. \tag{C.2}$$

Defining a square matrix

$$D_{(34),(12)} \equiv \delta_{(12),(34)} - V_{3214} \frac{n_{12}}{e_{12}}, \quad (e_3 \neq e_4, e_1 \neq e_2), \tag{C.3}$$

the $e_3 \neq e_4$ part of Eq. (C.2) is written as $Dw^{(10)} \doteq 0$. Because the quantities $w_{c12}^{(10)}$ do not vanish, we have $\mathrm{Det}[D] \doteq 0$. Thus D^T, the transpose matrix of D, has a zero eigenvalue. More accurately, D^T has an eigenvalue of order ω^2; because $\mathrm{Det}[D]$, the product of all eigenvalues of D^T, is of order ω^2. Assume that the eigenvector corresponding to this eigenvalue is η_{34}:

$$D^T \eta \doteq 0 \; \eta = 0 \quad \Rightarrow \quad \eta^T D \doteq 0. \tag{C.4}$$

C.2 Cubic Anharmonicity

Keeping only the constant terms of Eq. (2.14) with $(rs) = (20)$, we have

$$-2i\Lambda^{(30)} r_{12}^{(01)} \doteq e_{12} r_{12}^{(20)} - n_{12} w_{12}^{(20)} + 2[w^{(10)}, r^{(10)}]_{12}. \tag{C.5}$$

Calculating $w^{(20)}_{34}$ from Eq. (C.5), the $e_3 \neq e_4$ part is written as

$$D \cdot w^{(20)} \doteq C, \tag{C.6}$$

where D is defined in Eq. (C.3), C contains $\Lambda^{(30)}$ and lower-order quantities. Multiplying Eq. (C.6) from the left by η^T and using Eq. (C.4) we obtain

$$\Lambda^{(30)} \cdot \sum_{e_1 \neq e_2} \sum_{e_3 \neq e_4} \eta_{34} V_{3214} \frac{r^{(01)}_{12}}{e_{12}} \quad \doteq$$
$$i \sum_{e_1 \neq e_2} \sum_{e_3 \neq e_4} \eta_{34} V_{3214} \frac{[w^{(10)}, r^{(10)}]_{12}}{e_{12}} - \frac{1}{2} \sum_{e_1 = e_{1'}} \sum_{e_3 \neq e_4} \eta_{34} V_{31'14} [p, r^{(10)}]_{11'}, \tag{C.7}$$

where p is given by $n_{12} p_{12} = -i r^{(10)}_{12}$. Eq. (C.7) gives $\Lambda^{(30)}_c + O(\omega^2)$. Then $w^{(20)}_{12}$ is solved from Eq. (C.6) with an overall factor (temporarily call $\delta^{(20)}$) still undetermined.

Neglecting the $-i\omega^2 r^{(02)}$ term, $w^{(11)}_{12}$ (then $r^{(11)}_{12}$) are solved from Eq. (2.14) with $(rs) = (11)$, as a function of $\Lambda^{(12)}$ and $\delta^{(20)}$. We emphasize that in solving $w^{(11)}_{12}$ the coefficient matrix is actually not singular after combining $w^{(11)}_{21} = (w^{(11)}_{12})^*$ with $w^{(11)}_{12}$, because $w^{(11)}$ have symmetries different from $w^{(10)}$ in Eq. (C.2).

From Eq. (2.14) with $(rs) = (02)$, we obtain an equation $D \cdot w^{(02)} \doteq ...$ Multiplying it from the left by η^T we fix $\delta^{(20)}$ as a function of $\Lambda^{(12)}$. Then from the equation $D \cdot w^{(02)} \doteq ...$ we solve for $w^{(02)}_{12}$ as a function of $\Lambda^{(12)}$, with an overall factor $\delta^{(02)}$ still undetermined.

In summary, there remain two undetermined parameters in this order: $\Lambda^{(12)}$ and an overall factor $\delta^{(02)}$ in $w^{(02)}_{12}$. The latter is $Q^{(02)}$ in the factorizable force model (Sec. 3.2).

C.3 Quartic Anharmonicity

Similarly, we obtain from Eq. (2.14) with $(rs) = (30)$ and $(rs) = (21)$:

$$\begin{aligned}
\Lambda^{(40)} \cdot \sum_{e_1\neq e_2}\sum_{e_3\neq e_4}\eta_{34}V_{3214}\frac{r^{(01)}_{12}}{e_{12}} &\doteq \frac{i}{3}\Lambda^{(12)}\sum_{e_1=e_{1'}}\sum_{e_3\neq e_4}\eta_{34}V_{31'14}r^{(20)}_{11'} \\
-\Lambda^{(30)}\sum_{e_1\neq e_2}\sum_{e_3\neq e_4}\eta_{34}V_{3214}\frac{r^{(11)}_{12}}{e_{12}} &- \frac{i}{3}\Lambda^{(30)}\sum_{e_1=e_{1'}}\sum_{e_3\neq e_4}\eta_{34}V_{31'14}r^{(02)}_{11'} \\
&+\frac{i}{2}\sum_{e_1\neq e_2}\sum_{e_3\neq e_4}\eta_{34}V_{3214}\frac{[w^{(20)},r^{(10)}]_{12}+[w^{(10)},r^{(20)}]_{12}}{e_{12}} \\
&-\frac{1}{6}\sum_{e_1=e_{1'}}\sum_{e_3\neq e_4}\eta_{34}V_{31'14}([w^{(20)},r^{(01)}]_{11'}+[w^{(01)},r^{(20)}]_{11'}) \\
&-\frac{1}{3}\sum_{e_1=e_{1'}}\sum_{e_3\neq e_4}\eta_{34}V_{31'14}([w^{(11)},r^{(10)}]_{11'}+[w^{(10)},r^{(11)}]_{11'}). \qquad \text{(C.8)}
\end{aligned}$$

Eq. (C.8) gives $\Lambda_c^{(40)} + O(\omega^2)$. There is one unknown parameter $\Lambda^{(12)}$; quantities $(r/w)^{(20)}$ and $(r/w)^{(11)}$ depend implicitly on $\Lambda^{(12)}$. Those terms with the cubic anharmonicity $\Lambda^{(12)}$ would be small in the case of spherical nuclei, as shown in chapter 5.

In summary, this appendix fixes the cubic potential $\Lambda^{(30)}$ (C.7) and the quartic potential $\Lambda^{(40)}$ (C.8) near the critical point $\omega^2 \approx 0$, by considering the leading terms of the GDM equation of motion.

Appendix D

Mode Coupling

In many soft nuclei there exists a low-lying octupole (3^-) mode. It can interact strongly with the quadrupole (2^+) mode, and both of them should be kept in the collective subspace. For convenience we still use α_μ, π_μ for the quadrupole mode; and use $\hat{\alpha}_\mu$, $\hat{\pi}_\mu$ for the octupole mode. The collective bosonic Hamiltonian replacing Eq. (2.4) is

$$\begin{aligned} H = & \frac{\omega^2}{2}\sqrt{5}(\alpha\times\alpha)^0_0 + \frac{1}{2}\sqrt{5}(\pi\times\pi)^0_0 \\ & + \frac{\hat{\omega}^2}{2}\sqrt{7}(\hat{\alpha}\times\hat{\alpha})^0_0 + \frac{1}{2}\sqrt{7}(\hat{\pi}\times\hat{\pi})^0_0 \\ & + \frac{\Lambda^{(10|20)}}{2}\sqrt{7}(\alpha\times(\hat{\alpha}\times\hat{\alpha})^2)^0_0 + \ldots \end{aligned} \tag{D.1}$$

$\Lambda^{(10|20)}$ is the most important mode-coupling term in the case of soft vibrations with large amplitudes.

Following the procedure of chapter 2 and appendix C, we are able to determine the leading constant term of $\Lambda^{(10|20)}$ in a Taylor expansion over both ω^2 and $\hat{\omega}^2$ [see Eq. (C.1)]. Below we give the result in the quadrupole plus pairing model. The microscopic Hamiltonian

is:

$$H = \sum_1 (\epsilon_1 - \mu) a_1^\dagger a_1 - \frac{G}{4} \sum_{12} a_1^\dagger a_{\tilde{1}}^\dagger a_{\tilde{2}} a_2$$
$$+ \frac{1}{4} \sum_{1234} \sum_\mu (-\kappa q_{\mu 14}^\dagger q_{\mu 23} + \kappa q_{\mu 13}^\dagger q_{\mu 24} - \hat{\kappa} \hat{q}_{\mu 14}^\dagger \hat{q}_{\mu 23} + \hat{\kappa} \hat{q}_{\mu 13}^\dagger \hat{q}_{\mu 24}) a_1^\dagger a_2^\dagger a_3 a_4. \qquad \text{(D.2)}$$

Approximately, this Hamiltonian can be written as $H \approx \sum_1 (\epsilon_1 - \mu) a_1^\dagger a_1 - G P^\dagger P - \frac{1}{2}\kappa \sum_\mu Q_\mu^\dagger Q_\mu - \frac{1}{2}\hat{\kappa} \sum_\mu \hat{Q}_\mu^\dagger \hat{Q}_\mu$, the difference is in a one-body term originating from the $Q \cdot Q$ part. $\hat{\kappa}$ is the strength of the octupole force. The mean field is determined by the HFB equation. In the harmonic order the two modes do not mix, the octupole mode satisfies the same QRPA equation (5.18) and normalization condition (5.19) as the quadrupole mode, with necessary changes. In the next order we have the main result:

$$\Lambda^{(10|20)} \doteq 2\kappa Q^{(10)} (\hat{\kappa} \hat{Q}^{(10)})^2 \cdot \sum_{n_1 j_1 n_2 j_2 n_3 j_3} \sqrt{\frac{(2j_1+1)(2j_2+1)(2j_3+1)}{7}}$$
$$\cdot \begin{Bmatrix} 3 & 2 & 3 \\ j_1 & j_2 & j_3 \end{Bmatrix} \cdot \left[2\, \xi_{\|13}^{(1)\dagger}\ \hat{\xi}_{\|32}^{(1)\dagger}\ \hat{\eta}_{\|21}^\dagger + \eta_{\|13}^\dagger\ \hat{\xi}_{\|32}^{(1)\dagger}\ \hat{\xi}_{\|21}^{(1)\dagger} \right]. \qquad \text{(D.3)}$$

The octupole operator $\hat{q}$ connects single-particle levels with opposite parity, thus the intruder level becomes important. This may destroy in Eq. (D.3) symmetry with respect to the Fermi surface. Three-body forces will contribute to the $\Lambda^{(10|20)}$ term quite differently. The coexistence and interaction of soft quadrupole and octupole modes could be important to the search of mechanisms for many-body enhancement of the nuclear Schiff moment and the atomic electric dipole moment [29].

Appendix E

Odd-Mass Nuclei

In the odd-mass nuclei the coupling between the unpaired nucleon and the collective modes is important. An effective Hamiltonian can be derived straightforwardly within the GDM formalism. The "collective" subspace in this case is spanned by the direct product of the unpaired nucleon and the phonons

$$b_1^\dagger|C_n\rangle \equiv b_1^\dagger \otimes (A^\dagger)^n|\Phi\rangle \quad (1 \in \Omega,\ 0 \leq n \leq n_{max}), \tag{E.1}$$

where $b_1^\dagger$ is the quasi-particle creation operator (4.21), and $|\Phi\rangle$ is the quasi-particle vacuum. Within this subspace the effective Hamiltonian is calculated as

$$\begin{aligned} \langle C_i|H_{e(12)}|C_j\rangle &\equiv \langle C_i|b_1|H|b_2^\dagger|C_j\rangle \\ \mathring{=} \langle C_i|\Lambda_{(12)}^{(00)} + \Lambda_{(12)}^{(10)}\alpha + \Lambda_{(12)}^{(01)}\pi + \Lambda_{(12)}^{(20)}\frac{\alpha^2}{2} + \Lambda_{(12)}^{(02)}\frac{\pi^2}{2} + ...|C_j\rangle, \end{aligned} \tag{E.2}$$

where we substitute the nucleonic Hamiltonian (2.1), then use Eq. (2.8) and its generalization to three-body density matrix. In the "collective" subspace (E.1) we diagonalize the resulting

effective Hamiltonian H_e (E.2).

The above treatment could also be used in calculating the states of "single-particle" nature in even-even nuclei, as mentioned in CONCLUSION.

BIBLIOGRAPHY

BIBLIOGRAPHY

[1] A. Bohr and B. Mottelson, *Nuclear Structure* (Benjamin, New York, 1975), Vol. 2.

[2] L. Prochniak and S.G. Rohozinski, J. Phys. G: Nucl. Part. Phys. **36**, 123101 (2009). /Topical review./

[3] A. Arima and F. Iachello, Ann. Rev. Nucl. Part. Sci. **31**, 75 (1981); F. Iachello and A. Arima, *the Interacting Boson Model* (Cambridge Univ. Press, 1987).

[4] A. Kerman and A. Klein, Phys. Rev. **132**, 1326 (1963).

[5] S.T. Belyaev and V.G. Zelevinsky, Yad. Fiz. **11**, 741 (1970) [Sov. J. Nucl. Phys. **11**, 416 (1970)]; Yad. Fiz. **16**, 1195 (1972) [Sov. J. Nucl. Phys. **16**, 657 (1973)]; Yad. Fiz. **17**, 525 (1973) [Sov. J. Nucl. Phys. **17**, 269 (1973)].

[6] V.G. Zelevinsky, Prog. Theor. Phys. Suppl. **74-75**, 251 (1983).

[7] M.I. Shtokman, Yad. Fiz. **22**, 479 (1975) [Sov. J. Nucl. Phys. **22**, 247 (1976)].

[8] V.G. Zelevinsky, Nucl. Phys. **A344**, 109 (1980).

[9] V.G. Zelevinsky, Nucl. Phys. **A337**, 40 (1980).

[10] P.N. Isaev, Yad. Fiz. **32**, 978 (1980) [Sov. J. Nucl. Phys. **32**, 5056 (1980)]; Yad. Fiz. **34**, 717 (1981) [Sov. J. Nucl. Phys. **34**, 399 (1981)].

[11] A. Klein and A.S. Umar, Phys. Rev. C **35**, 1672 (1987).

[12] L.Y. Jia, Phys. Rev. C **84**, 024318 (2011).

[13] L. Y. Jia and V. G. Zelevinsky, Phys. Rev. C **84**, 064311 (2011).

[14] L. Y. Jia and V. G. Zelevinsky, Phys. Rev. C **86**, 014315 (2012).

[15] V. G. Zelevinsky, Int. J. Mod. Phys. **E2**, 273 (1993).

[16] H. J. Lipkin, N. Meshkov and A. J. Glick, Nucl. Phys. **62**, 188 (1965).

[17] A. Klein and E.R. Marshalek, Rev. Mod. Phys. **63**, 375 (1991).

[18] O. K. Vorov and V. G. Zelevinsky, Nucl. Phys. **A439**, 207 (1985).

[19] S. T. Belyaev, Nucl. Phys. **64**, 17 (1965).

[20] A. Bohr, B. R. Mottelson and D. Pines, Phys. Rev. **110**, 936 (1958).

[21] S. T. Belyaev, Mat. Fys. Medd. Kgl. Dan. Vidensk. Selsk. **31**, No. 11 (1959).

[22] NuShellX@MSU, B. A. Brown and W. D. M. Rae,
http://www.nscl.msu.edu/ brown/resources/resources.html

[23] B. A. Brown, N. J. Stone, J. R. Stone, I. S. Towner, and M. Hjorth-Jensen, Phys. Rev. C **71**, 044317 (2005).

[24] T. Trivedi, P. C. Srivastava, D. Negi, and I. Mehrotra, Int. J. Mod. Phys. **E21**, 1250049 (2012).

[25] J. Blomqvist and A. Molinari, Nucl. Phys. **A106**, 545 (1968).

[26] National Nuclear Data Center, http://www.nndc.bnl.gov/.

[27] B. G. Carlsson, J. Toivanen, and A. Pastore, Phys. Rev. C **86**, 014307 (2012).

[28] L. S. Kisslinger and R. A. Sorensen, Rev. Mod. Phys. **35**, 853 (1963).

[29] N. Auerbach and V. Zelevinsky, J. Phys. G: Nucl. Part. Phys. **35**, 093101 (2008).